

1 **State-of-the-art hydrological datasets exhibit low water balance**
2 **consistency globally**

3 **Hao Huang¹, Junguo Liu^{1,2}, Aifang Chen³, Melissa Ruiz-Vásquez^{4,5}, René Orth⁵**

4 ¹School of Environmental Science and Engineering, Southern University of Science and Technology,
5 Shenzhen, China

6 ²Henan Provincial Key Laboratory of Hydrosphere and Watershed Water Security, North China University of
7 Water Resources and Electric Power, Zhengzhou, China

8 ³School of Environment and Civil Engineering, Dongguan University of Technology, Dongguan, China

9 ⁴Max Planck Institute for Biogeochemistry, Jena, Germany

10 ⁵Faculty of Environment and Natural Resources, University of Freiburg, Freiburg, Germany

11

12 *Correspondence to:* Junguo Liu (junguo.liu@gmail.com)

13

14 **Abstract**

15 The proliferation and diversification of hydrological datasets have significantly advanced
16 hydrological research. However, the coherence across these datasets remains poorly understood,
17 hindering the comparability of findings derived from different data sources and variables. Here,
18 we demonstrate that state-of-the-art hydrological datasets exhibit overall low consistency when
19 evaluated through the lens of water balance ~~–~~ specifically, the relationship between variations in
20 soil moisture and the difference between precipitation, evapotranspiration, and runoff. Our
21 analysis reveals that satellite-based precipitation datasets generally show the highest consistency,
22 while gauge-based datasets perform better in densely monitored regions of the Northern
23 Hemisphere. For evapotranspiration, runoff, and soil moisture, reanalysis datasets demonstrate
24 broader areas of higher consistency compared to gauge- or satellite-based products. Spatial
25 patterns of consistency [for most assessed datasets](#) are strongly influenced by aridity and
26 temperature, which affect measurement and modelling accuracy. Notably, dataset consistency has
27 improved significantly in northern mid-latitudes over recent decades, likely reflecting
28 advancements in observational technologies and the effects of climate warming. These findings
29 underscore the importance of continued efforts to enhance dataset coherence and reliability for
30 robust hydrological assessments.

31

32 **1 Introduction**

33 Over the past decades, the advancement of hydrological science and interconnected water-related
34 research fields was accompanied by the emergence of datasets that depict the spatiotemporal
35 changes of variables in the water cycle (Tang et al., 2024; Zarei and Destouni, 2024;
36 Gebrechorkos et al., 2024; Douville et al., 2021; Oki and Kanae, 2006; Wang-Erlandsson et al.,
37 2022; Mehta et al., 2024; Markonis et al., 2024). At the same time, understanding the consistency
38 across the increasing suite of datasets is crucial not only for research on the responses and
39 interactions within hydrology, but also for practitioners and management in terms of regional
40 water scarcity (Mekonnen and Hoekstra, 2016; Mehta et al., 2024), ecosystem function and

Deleted: –

Deleted: , while vegetation cover further modulates the performance of soil moisture datasets

44 water availability (Denissen et al., 2022), and the Earth system resilience (Wang-Erlandsson et
45 al., 2022; Jaramillo and Destouni, 2015). Nevertheless, the water balance consistency among
46 different suites remains largely unknown, while current studies mostly detail the dataset
47 performance in terms of accuracies against observations and/or reference data, modeling
48 behaviors, or water and energy balance closure (Tang et al., 2024; Gebrechorkos et al., 2024; Pan
49 et al., 2020; Zarei and Destouni, 2024; Abolafia-Rosenzweig et al., 2021; Zhang et al., 2016).

50 Gridded hydrological datasets are derived based on different types of observations and methods,
51 such as (i) spatial interpolation based on gauge/station/*in-situ* measurements (Harris et al., 2020),
52 (ii) radiative transfer modelling based on satellite measurements (McCabe et al., 2017), (iii) land
53 surface modelling with integrated data assimilation of hydrological and other variables (Muñoz-
54 Sabater et al., 2021). Meanwhile, datasets also could be developed based on a combination of
55 these approaches and observations (Beck et al., 2019; Yao et al., 2014), and machine-learning
56 methods started to be implemented for parameterization (Ashouri et al., 2015). In this context,
57 each of these approaches is characterized by inherent advantages and disadvantages. For
58 example, in the case of precipitation (P), gauge-based datasets are based on ground truth but at
59 the same time they are influenced by errors related to wind and air flow anomalies around the
60 gauges, by the spatial distribution of gauges which potentially misses some of the spatial
61 heterogeneity of precipitation patterns, and by uncertainties in spatial interpolation (Lanza et al.,
62 2022; Mishra and Coulibaly, 2009; La et al., 2002). By contrast, satellite-based P datasets can
63 capture spatial patterns more consistently (Tang et al., 2022; Ashouri et al., 2015; Funk et al.,
64 2015), but have difficulties in estimating P amounts arriving at the surface. Further, reanalysis
65 datasets based on land surface models show strengths in addressing temporal gaps caused by
66 missing records and incomplete observation periods (Hersbach et al., 2020; Gelaro et al., 2017),
67 but they suffer from inadequate or incomplete consideration of land surface processes that affect
68 hydrological dynamics.

69 With the developing observation networks and data synthesis (Dorigo et al., 2021; Pastorello et
70 al., 2020; Do et al., 2018), machine-learning algorithms present an alternative opportunity
71 instead of interpolation to produce seamless observation-based datasets globally for
72 evapotranspiration (ET), runoff (R), and soil moisture (SM) datasets (Nelson et al., 2024; Ghiggi
73 et al., 2019; O and Orth, 2021). Although Penman-Monteith and the simpler Priestley-Taylor
74 models are still the key physical algorithms to estimate ET through remote sensing, the relevant
75 products tend to leverage recent advances in satellite data and climate reanalysis (Fisher et al.,
76 2008; Miralles et al., 2025; Zhang et al., 2019). Differently, satellite-based SM datasets follow
77 different technical roadmaps, such as merging retrievals from various sensors (Gruber et al.,
78 2019) or assimilating radiometer observations into land surface modeling (Reichle et al., 2019).
79 In this way, the latter additionally provides an SM -constrained R dataset (Reichle et al., 2019). At
80 the same time, there are updated parametrizations for the land surface model in reanalysis to
81 better describe the soil water balance and hydrological cycle (Hirschi et al., 2025; Muñoz-
82 Sabater et al., 2021). It has been documented that those technical discrepancies could cause
83 datasets' performance in terms of agreement with observations, while the influence of
84 environmental factors remains unclear (Markonis et al., 2024; Tang et al., 2024).

85 As a result of the different derivation approaches and the influence of environmental factors,
86 disagreements between hydrological datasets remain (Hirschi et al., 2025; Markonis et al., 2024;
87 Sun et al., 2018). These uncertainties limit the fundamental understanding of patterns, changes,
88 and variabilities of water balance components (Markonis et al., 2024; Wang et al., 2024; Han et

Deleted: Dorigo et al., 2011; Pastorello et al., 2020; Do et al., 2018; ...

Deleted: Cooley et al., 2022; Mccabe

Deleted:).

Deleted: to

Deleted: inaccurate

Deleted: affecting

Deleted: From this aspect,

Deleted: data, firstly happening

Deleted: estimating P (Ashouri et al., 2015) and recently also being applied to

Deleted: variables

101 al., 2024; Douville et al., 2021; Greve et al., 2014; Zhang et al., 2024a; Denissen et al., 2022).
102 The scarcity of observations across time, space, and hydrological variables hinders a
103 comprehensive analysis of datasets' performance and reliability. However, observations are not
104 our only source of knowledge about Nature, but known physical laws also provide information.
105 This way, for example the water balance equation can be used to evaluate the consistency across
106 combinations of hydrological datasets, a question which has remained largely unclear because
107 assessments are usually specific to individual datasets (Zarei and Destouni, 2024; Abolafia-
108 Rosenzweig et al., 2021). Such a combinatorial and factorial analysis requires (i) gridded
109 datasets of all involved variables and (ii) independence between them in the sense that they are
110 not derived with, e.g., the same model or approach which inherently enforces water balance
111 closure. Thanks to the recent emergence of many hydrological datasets (Muñoz-Sabater et al.,
112 2021; Ghiggi et al., 2019; Miralles et al., 2025), these requirements are now met, opening a novel
113 opportunity for hydrological dataset evaluation.

114 In this study, we evaluate the water balance consistency across a comprehensive set of P , ET , R
115 and SM datasets. This encompasses gauge/station-based, satellite-based and reanalysis-based
116 datasets, and offers 8,294 combinations of water balance-variables from independently derived
117 datasets (Fig. 1a). For each combination, we evaluate adjusted R^2 as the performance of linear
118 regression of temporal changes in $P-ET-R$ against changes in SM (ΔSM) to determine its water
119 balance consistency, [since \$R^2\$ corresponds to the coefficient of determination](#). Then, combining
120 an individual dataset with all possible combinations of datasets for the remaining water balance-
121 variables we can assess its performance through the average of the R^2 scores obtained for all
122 considered combinations. This way, the common limitations and strengths of different
123 derivation-based datasets for each variable (i.e., P , ET , R , and SM) are distinguished across space
124 and time. In addition to determining the performance of a large set of considered hydrological
125 datasets across the globe, we also evaluate the resulting spatial patterns for possible causes in
126 order to provide guidance for further dataset development.

127

128 **2 Materials and Methods**

129 **2.1 Data and Independent combinations**

130 We utilized 20 P datasets, 11 ET datasets, 7 R datasets, and 9 SM datasets to obtain respective
131 monthly values across the global land area, where the P , ET , and R values are monthly amounts
132 and ΔSM values are the soil moisture differences between the last day and the first day of each
133 month. According to their sources, these datasets were summarized into three categories:

- 134 • Gauge/station-based products: CPC (Xie et al., 2010), CRU TS v4.06 (Harris et al.,
135 2020), UDel v5.01 (Legates and Willmott, 1990), EM-EARTH (Tang et al., 2022), GPCC
136 v2022 (Schneider et al., 2022), and PREC/L (Chen et al., 2002) for P , X-BASE (Nelson
137 et al., 2024) for ET , GRUN (Ghiggi et al., 2019) for R , as well as SoMo.ml (O and Orth,
138 2021) for ΔSM .
- 139 • Satellite-based products: CHIRPS v2.0 (Funk et al., 2015), CMAP (Xie and Arkin, 1997),
140 CMORPH v1 (Xie et al., 2017), GPCP(M) v2.3 (Adler et al., 2018), GPCP(D) v1.3
141 (Huffman et al., 2001), GPM IMERG v07 (Huffman et al., 2023), PERSIANN-CDR
142 (Ashouri et al., 2015), MSWEP v2.8 (Beck et al., 2019) for P , MODIS (Running et al.,
143 2021), PT-JPL (Fisher et al., 2008), PML-v2 (Zhang et al., 2019), GLASS (Yao et al.,
144 2014) for ET , GLEAM v4.1 (Miralles et al., 2025) for both ET and ΔSM , SMAP L4 v7

Deleted: .

146 (Reichle et al., 2019) for both R and ΔSM , as well as ESA CCI v08.1 (Gruber et al., 2019)
 147 for ΔSM .
 148 • Reanalysis products: 20CR v3 (Slivinski et al., 2021), JRA-55 (Japan Meteorological
 149 Agency, 2013), ERA5 (Hersbach et al., 2020), NCEP-NCAR R1 (Kistler et al., 2001),
 150 and NCEP-DOE R2 (Kanamitsu et al., 2002) for P , MERRA-2 (Gelaro et al., 2017) for
 151 P , ET , R , and ΔSM , as well as GLDAS-2.0 (Rodell et al., 2004), GLDAS-2.1 (Rodell et
 152 al., 2004), GLDAS-2.2 (Li et al., 2019), ERA5-land (Muñoz-Sabater et al., 2021) for ET ,
 153 R , and ΔSM .

154 All datasets were either provided at or resampled to 0.25-degree resolution by bilinear
 155 interpolation, and their temporal coverage spans Jan-2000 to Dec-2022. Various components of
 156 GLDAS (i.e., -2.0, -2.1, and -2.2) were used here because they are based on different forcings,
 157 models, and data assimilation strategies (see more details in Tables S1–S4). The ΔSM from
 158 different datasets were the depth-weighted averages of their available soil layers (Li et al.,
 159 2023a). SoMo.ml ΔSM covers 0–50 cm related to the commonly observed depths in *in-situ*
 160 measurements; ESA CCI ΔSM represents the top surface layer (of < 2 cm thickness) captured by
 161 satellite observations; GLEAM ΔSM , SMAP ΔSM , and MERRA-2 ΔSM represent a root zone
 162 layer of 0–100 cm; and GLDAS-2.0/2.1/2.2 and ERA5-land ΔSM cover deeper depths (> 100
 163 cm). Despite differences in depth, the ΔSM was assumed to capture the variability of $P - ET - R$
 164 in the water balance, on the basis that its variability accounts for a large portion of the variability
 165 in terrestrial water storage (Freedman et al., 2014). In this context, a suite of P , ET , R , and SM
 166 datasets forms a considered combination, such as

$$P_{CPC}, ET_{X-BASE}, R_{GUN}, \text{ and } \Delta SM_{SoMo.ml}$$

168 Among the considered datasets as listed above, 13,860 combinations (that is $20 \times 11 \times 7 \times 9$ for P ,
 169 ET , R , and S) were initially available. However, considering the temporal availability and the
 170 dependence between dataset sources of different water balance components, parts of
 171 combinations were excluded by three rules:

- 172 1) The combinations with short overlapping time periods cannot be considered. In particular,
- 173 • SMAP L4 products have only one year overlap (i.e., 2015) with 20CR v3, so the
 - 174 combinations with P from 20CR v3 and R and/or ΔSM from SMAP were not considered;
 - 175 • The combinations with GRUN R (covering until 2014) and R and/or ΔSM from SMAP
 - 176 (starting from 2015) were not available;
 - 177 • The combinations with water balance components from GLDAS-2.0 (also covering until
 - 178 2014) and SMAP were not available;
 - 179 • The combinations with SMAP L4 products and either PT-JPL or UDel v5.01 (covering
 - 180 until 2017) were not considered.
- 181 2) The combinations with water balance components from the same dataset source were not
 182 considered, which include the combinations with GLEAM ET and ΔSM , the combinations with
 183 SMAP ET and ΔSM , and the combinations with any two or more variables from MERRA-
 184 2/GLDAS/ERA5-land. In this perspective, since the difference between ERA5 and ERA5-land
 185 was mainly because of the non-linear dynamical downscaling technique (Muñoz-Sabater et al.,
 186 2021), the combinations with ERA5 P and ERA5-land $ET/R/\Delta S$ were also not considered.
- 187 3) If a dataset was driven by another dataset, the water balance components from these two
 188 datasets were also not considered in combination. In particular:

Deleted: the
 Deleted: in
 Deleted: in
 Deleted: linear
 Deleted: coverages are within the period of

Deleted: different depths
 Deleted: record
 Deleted: –
 Deleted: constitutes

- 198 • GRUN was driven by GSWP3, a dynamically downscaled and bias-corrected version of
199 the 20CR, so the combinations with 20CR P and GRUN R were excluded;
- 200 • SoMo.ml was driven by meteorological data from ERA5, so the combinations with ERA5
201 P and SoMo.ml ΔSM were excluded;
- 202 • PML-v2 used the GLDAS-2.1 meteorological forcings, which includes GPCP(D) v1.3, so
203 the combinations with GPCP(D) P and PML ET , as well as those with GPCP(D) P and
204 GLDAS-2.1 ET , were excluded;
- 205 • GLEAM v4.1 used P from MSWEP v2.8 as one of the inputs, so the combinations with
206 MSWEP P and GLEAM $ET/\Delta SM$ were excluded;
- 207 • The [input](#) P for SMAP L4 was from CPC and GPCP(M), and therefore, the combinations
208 with CPC/GPCP(M) P and SMAP $R/\Delta SM$ were excluded;
- 209 • Since the land surface component of MERRA-2 bias adjusted P by using CPC, CMAP,
210 and GPCP(M), the combinations with CPC/CMAP/GPCP(M) P and MERRA-2
211 $ET/R/\Delta SM$ were excluded;
- 212 • The GLDAS-2.2 was forced with the meteorological analysis fields from the European
213 Centre for Medium-Range Weather Forecasts (ECMWF) Integrated Forecasting System
214 (IFS)(Rui et al., 2022), which includes ERA5, so the combinations with ERA5 P and
215 GLDAS-2.2 $ET/R/\Delta SM$ were excluded.

Deleted: inputted

216 At the same time, there are different levels of (in)dependence such that the decision on whether
217 or not to consider certain datasets as independent is not always straightforward. The following
218 cases are not fully independent but [are](#) considered sufficiently independent for the context of our
219 study:

- 220 • The datasets driven by similar forcings, such as SoMo.ml ΔSM and ERA5-land ET and R ,
221 are considered to form independent combinations;
- 222 • MSWEP generated based on a group of P datasets including ERA5 is considered
223 sufficiently independent from the ERA5-land ET , R , and ΔSM ;
- 224 • ESA CCI ΔSM which was assimilated into GLEAM ΔSM is considered independent from
225 GLEAM ET .

226 After applying these exclusion rules, there remained 8,294 independent combinations.

227 2.2 Performance assessment in terms of water balance consistency

228 [Under our water balance assumption, we build a linear regression model in each grid cell of each](#)
229 [considered combination of hydrological datasets, considering all available months, and assess its](#)
230 [adjusted \$R^2\$ score:](#)

Deleted: For

Deleted: we assess adjusted R^2 scores in water balance in each grid cell through a linear regression model

$$231 (\mathbf{P} - \mathbf{ET} - \mathbf{R})_s = k \cdot \mathbf{\Delta SM}_s \quad (1)$$

Deleted: -

Deleted: -

232 where s is the spatial index (grid cell) and k is the proportionality factor. Note that this is not
233 supposed to equal to 1 in our context because of the differences in units between the left side of
234 the equation (mm for \mathbf{P} , \mathbf{ET} , and \mathbf{R}) and the right side ($\text{m}^3 \cdot \text{m}^{-3}$ for $\mathbf{\Delta SM}$). The linear regression
235 model lets us avoid the conversion of $\mathbf{\Delta SM}$ unit from $\text{m}^3 \cdot \text{m}^{-3}$ to mm, reducing uncertainties from
236 considering soil moisture datasets with different soil depths. \mathbf{P} , \mathbf{ET} , \mathbf{R} , and $\mathbf{\Delta SM}$ are $M \times 1$
237 vectors, where M is the number of months. We removed the models with M smaller than 36 to
238 ensure enough input data. The adjusted R^2 score for each model was used to represent the ability
239 of each combination of datasets to describe the variability in water balance at each grid point.
240 Since the water balance is a physical law that should be obeyed according to mass balance, the

247 ability of describing variability here is attributed to the performance of each combination for
248 each grid cell.

249 [Different](#) independent combinations have different temporal coverages (i.e., different M), [so](#) we
250 analyzed whether the varying M would affect the accuracy results. For this purpose, a fixed study
251 period [from](#) Feb-2003 to Dec-2014 (where M is fixed to be 143) was selected. We calculated the
252 water balance [consistency](#) based on the adjusted R^2 score, [for](#) all available independent
253 combinations [with](#) this fixed M . We compared the R^2 values between varying M and fixed M for
254 each considered combination by calculating their linearly regressed R^2 scores and slopes. Most
255 of the regressed R^2 and slopes are distributed between 0.9 and 1 (Fig. S1). This indicates that the
256 considered time period has no significant influence on the resulting water balance [consistency](#).
257 Therefore, we assessed the performance [in terms of water balance consistency](#) across different
258 time periods for different combinations of datasets, depending on their temporal coverage and
259 overlap (ensuring a minimum overlap of 3 years). This allows us to involve a larger number of
260 combinations compared to a fixed M , while we also provided the results calculated based on the
261 combinations used in the following temporal changes analysis, which have only large and less
262 varying M (Fig. S2).

263 In [the](#) next step, the overall performance in terms of water balance consistency for each
264 individual dataset in each grid cell was inferred from the averaged R^2 across all combinations of
265 datasets containing the respective dataset. In other words, the performance of each individual
266 dataset is assessed through the R^2 scores in water balance for describing variability when
267 combining it with all suitable combinations of state-of-the-art datasets for the other water
268 balance components.

269 Since the performance inferred from water balance consistency is based on the ability to describe
270 variability in water balance, different temporal resolutions directly affected magnitudes and
271 frequencies of the variability (Maurer and Hidalgo, 2008). Accordingly, we repeated the above
272 calculations for the datasets available at daily and yearly resolutions, where 3,647 and 8,294 (the
273 same as monthly) independent combinations were considered, respectively (Text S1–S2). [In](#)
274 [addition, unconsidered water variables, like glacier, snow, and surface water storage, might](#)
275 [introduce bias into our water balance assumption, leading to a nonlinear response of \$\Delta SM\$ to \$P\$ -](#)
276 [\$ET\$ - \$R\$. We thereby used terrestrial water storage from GRACE instead of \$SM\$ in equation \(1\) to](#)
277 [evaluate the performance of the \$P\$, \$ET\$, and \$R\$ datasets, based on their combinations with GRACE](#)
278 [data \(Text S3\). In this case, the number of combinations is decreased by one order of magnitude](#)
279 [\(933 remained\), but ranking results are similar to using \$\Delta SM\$ \(Fig. S3\).](#)

280

281 2.3 Potential influence factors on dataset performance

282 To further understand how the global spatial patterns of each dataset's performance (Figs.
283 [S4–S7](#)) were influenced, we considered a set of potential influence factors of the spatial patterns:
284 soil texture, aridity index, tree cover fraction, area equipped for irrigation, [artificial impervious](#)
285 [area](#), monthly mean temperature, observation density, and [potential influence of lateral flow](#). For
286 the first [six](#) factors, we calculated them for each independent combination because the factors are
287 changing from dataset to dataset, and then obtained the averages for each dataset through all the
288 considered combinations that include this dataset. In detail,

- 289 • Soil clay content was used to indicate soil texture influence, since small particles and

Deleted: Since different

Deleted: of

Deleted: degree of

Deleted: closure, evaluated

Deleted: of

Deleted: for

Deleted: degree of

Deleted: closure

Deleted: a

Deleted: S3–S6

Deleted: topography.

Deleted: five

302 large surface areas can create small pore sizes to hold water tightly, affecting *SM*
 303 conditions and through local water cycles to influence other water [balance components](#)
 304 (Cleophas et al., 2022). The clay contents were provided by the Harmonized World Soil
 305 Database version 2.0 (HWSD v2.0) (Nachtergaele et al., 2023) for seven soil layers, and
 306 the layers used for each independent combination were selected according to the depth of
 307 *SM* dataset in that combination and depth-weighted for a whole layer.

- 308 • Regarding the aridity index, we used the multi-year averages of *ET* and divided them by
 309 those of *P* to obtain an aridity index map for each independent combination (O and Orth,
 310 2021; Li et al., 2022).
- 311 • The tree cover fraction from NASA Vegetation Continuous Fields Version 1 data product
 312 (Hansen and Song, 2018).
- 313 • Area equipped for irrigation from Mehta et al. (2024) [was averaged among the available](#)
 314 [periods for each independent combination.](#)
- 315 • [Global artificial impervious area from Gong et al. \(2019\) was also averaged among the](#)
 316 [available periods for each independent combination.](#)
- 317 • The monthly mean 2m air temperature was averaged based on the daily average
 318 temperature from ERA5 and calculated for each month in each considered combination.
- 319 • Unlike the upper factors, the observation density is different from variable to variable, not
 320 from combination to combination. We counted the number of stations/sites for different
 321 observation networks of the water variables: CPC global stations for *P*, eddy covariance
 322 sites in FLUXNET2015 (Pastorello et al., 2020) and AmeriFlux for *ET*, streamflow
 323 stations in the Global Streamflow Indices and Metadata Archive (GSIM) (Do et al., 2018)
 324 for *R*, and sites of *in-situ* measurement in the International Soil Moisture Network
 325 (ISMN) (Dorigo et al., 2021) and the National Center for Monitoring and Early Warning
 326 of Natural Disasters of Brazil (CEMADEN) (Zeri et al., 2020) for *SM*. Here, we referred
 327 to Ruiz-Vásquez et al. (2022) to sum up the stations/sites located in each grid cell and its
 328 eight neighboring grid cells (Fig. S8).
- 329 • [The global impact of lateral flow has been evaluated by Miguez-Macho and Fan \(2025\),](#)
 330 [where the differences of \(*P* + lateral flow\)/PET and *P*/PET \(with PET as the potential](#)
 331 [evapotranspiration\) represent the influence of subsidies by rivers and groundwater on](#)
 332 [regional water cycles \(Fig. S9\).](#)

333 An explainable machine learning method was applied for quantitative attribution (Li et al., 2022)
 334 in order to determine the relative roles of the considered factors for the resulting global spatial
 335 patterns of each dataset's performance. For each dataset, we trained one random forest model,
 336 where the global performance map was the target variable, the seven maps of the above-
 337 described factors were the predictors, and a common hyperparameter setting (numbers of
 338 estimators: 100; maximum features: 30%) was used (Li et al., 2022). Before training, the
 339 correlation matrix of the seven predictors [was calculated](#) for each random forest model to [assess](#)
 340 potential collinearity. Since the correlations are within a range of -0.2–0.5 (Figs. S10–S13 for *P*,
 341 *ET*, *R*, and *SM* datasets, respectively), collinearity is not a major issue [affecting](#) our model
 342 predictions (Dormann et al., 2012). The performance of random forest models was determined
 343 by the cross-validation out-of-bag R^2 , which mainly distributes around 0.8 for all the trained
 344 models and therefore indicates the usefulness of these models for the following attribution (Fig.
 345 S14). Then, SHapley Additive exPlanations (SHAP) feature importance was calculated to
 346 quantify the marginal contributions of predictors to each dataset's overall accuracy (Li et al.,
 347 2023a), and we identified the relative importance among predictors by ranking their global

Deleted: variables

Deleted:

Deleted: were

Deleted:

Deleted: 2011

Deleted: S7).

Deleted: <#>The topography information is represented by the standard deviation of 15 arc-second elevation (Noaa National Centers for Environmental Information, 2022) within each 0.25° grid cell.

Deleted: was calculated

Deleted: evaluate the

Formatted

Formatted

Formatted

Deleted: between predictors.

Deleted: 5

Deleted: 6

Deleted: S8–S11

Deleted: to affect

Deleted: S12

366 averaged absolute SHAP values (Li et al., 2023b).

367 2.4 Temporal changes in dataset performance

368 Since the temporal coverages of independent combinations are inconsistent, the independent
369 combinations with less than two-thirds of available monthly data for either the first period of
370 Jan-2000 to Dec-2010 or the second period of Jan-2011 to Dec-2022 were removed in the
371 temporal changes analysis. The remaining independent combinations ($n = 2,589$) were used to
372 separately calculate water balance consistency for the first and second periods. The overall
373 performance in terms of water balance consistency was calculated for the first or second period
374 of each dataset by averaging the respective period's adjusted R^2 scores across all independent
375 combinations of the datasets considered in this study. In this way, the temporal change in
376 performance for each dataset was obtained by subtracting the overall performance of the first
377 period from that of the second period.

378 To account for the uncertainties of these temporal changes, bootstrap confidence intervals
379 (Kulesa et al., 2015) were calculated for the performance in both the first and the second periods
380 of the 2,589 independent combinations. For each of these independent combinations, whose
381 number of available monthly data for the first and the second periods is denoted as M_1 and M_2 ,
382 respectively, we obtained 100 random samples for the first/second period with replacement. The
383 amount of data in one sample is M_1 for the first period and M_2 for the second period, and 100
384 samples indicate that 100 adjusted R^2 scores were calculated for the first/second period based on
385 equation (1). Accordingly, a bootstrap distribution for the first/second period with 100 samples
386 was obtained, and its confidence interval was evaluated by the 5th and 95th percentiles. When the
387 5th percentile of the second period is higher than the 95th percentile of the first period, or the 95th
388 percentile of the second period is lower than the 5th percentile of the first period, the change in
389 performance of this independent combination from the first to the second period is significant.
390 Finally, grids in the map of temporal changes in performance for each dataset were masked by
391 n/a (i.e., not available) if they did not have over 50% independent combinations showing
392 significant changes.

393

394 3 Results

395 3.1 Water balance consistency of considered datasets

396 Fig. 1b-e summarizes the performance of considered datasets in terms of their water balance
397 consistency, based on monthly calculations (see Methods). Colors distinguish gauge-based,
398 satellite-based and reanalysis datasets. Overall, the R^2 scores are fairly low, indicating prevailing
399 inconsistencies across considered datasets in terms of the water balance. From the combinations
400 with top ten performance, it is likely that the P from PERSIANN-CDR, ET from PT-JPL, R from
401 GRUN, and SM from GLDAS-2.1 would contribute to high water balance consistency (Fig.
402 [S15](#)).

403 For P datasets, the overall performance of satellite-based datasets is generally higher than gauge-
404 based and reanalysis datasets, where the CHIPRS v2.0 and PERSIANN-CDR show the highest
405 global medians (Fig. 1b). This is related to their limited spatial coverage omitting high-latitude
406 regions with typically low water balance consistency (Fig. [S4](#)), while for 50°S–50°N,
407 PERSIANN-CDR, GPM IMERG v07, and MSWEP v2.8 show the highest medians (Fig. 1b).
408 Besides, GPM IMERG v07 and MSWEP v2.8 exhibit the largest areas with the best performance

Deleted:

Deleted: the

Deleted: period

Deleted: the

Deleted: period separately

Formatted

Formatted

Formatted

Formatted

Formatted

Deleted: the

Deleted: periods

Formatted

Formatted

Deleted: among

Deleted: the

Formatted

Formatted

Deleted: are

Deleted: S13

Deleted: S3

421 across datasets. Fig. 2 maps the types of datasets with the highest water balance consistency for
422 each considered variable. It shows that given the comparatively good performance of GPM
423 IMERG v07 and MSWEP v2.8, satellite-based precipitation dataset types perform best across
424 most of the globe, particularly in the tropics and subtropics (Fig. S16 and Fig. 2a). Gauge-based
425 *P* datasets perform best in high-latitude regions which in the Northern Hemisphere are
426 characterized by abundant *in-situ* observations (Fig. S8).

427 *ET* and *R* datasets show similar global patterns and medians of overall performance among the
428 different dataset types (Figs. S5–S6 and Fig. 1cd). However, for the spatial patterns, PT-JPL and
429 GLDAS-2.2 have distinctly larger areas with the best performance compared to other *ET* datasets
430 (Fig. S16b), leading to comparable best-performance areas between satellite-based and reanalysis
431 *ET* datasets (Fig. 2b). Similarly, gauge-based and reanalysis *R* datasets show the largest areas
432 with the best performance (Fig. 2c), where GRUN and ERA5-land datasets are the respective
433 main contributors (Fig. S16c).

434 Among *SM* datasets, SoMo.ml and ESA CCI v08.1 have the lowest global medians of overall
435 performance. This is because they only represent the surface layers instead of the entire soil
436 column (Fig. 1e). Meanwhile, the *SM* datasets with simulations of deep soil layers generally
437 performed better in most global regions, such as the reanalysis and GLDAS-2 products (Fig. 2d
438 and Fig. S16d).

439 Additionally, we calculated our analysis at daily and annual time scales. Results indicate
440 substantially less water balance consistency with the lowest R^2 scores at the annual scale (Fig.
441 1b–e). However, different temporal resolutions did not alter the relative ranking patterns among
442 the datasets (Fig. 1b–d), except for *SM* whose memory is likely to be more sensitive to the
443 varying resolutions (Fig. 1e).

444

Deleted: S14

Deleted: S7

Deleted: S4–

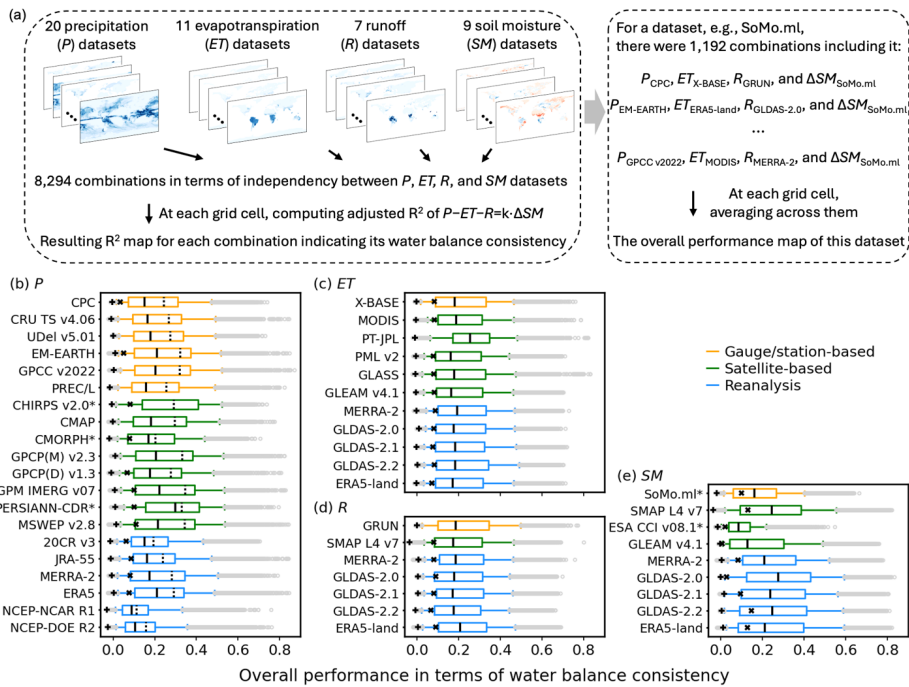
Deleted: S14b

Deleted: S14c

Deleted: layer

Deleted: S14d).

Deleted: and Fig. S15

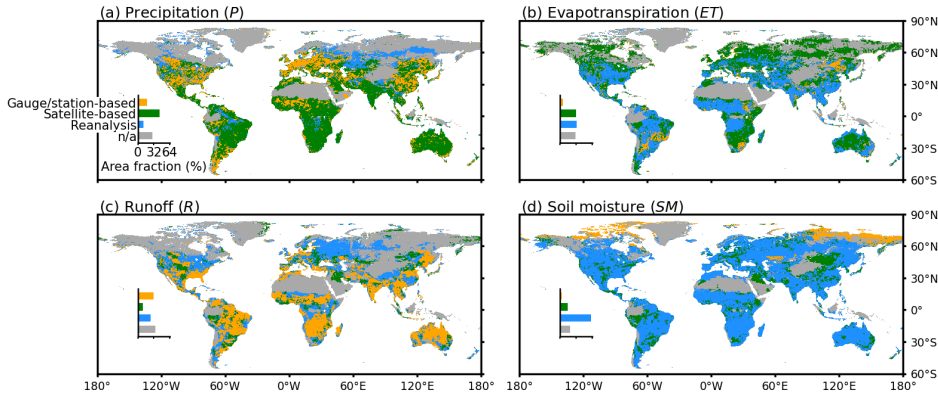


453

454 **Fig. 1. Illustration of water-balance approach and calculated performance of considered**
 455 **datasets.** (a) Performance is determined based on R^2 scores measuring consistency of each
 456 dataset when combined with all independent datasets in terms of the water balance (Methods).
 457 (b–e) The boxplots summarize the performance of considered datasets. Colors indicate the type
 458 of each dataset. Each box shows the median value, as well as the 5th, 25th, 75th, and 95th
 459 percentiles of the global pattern of water balance consistency derived from monthly data. Median
 460 results for performing the analysis with daily and annual data are indicated through crosses (×)
 461 and pluses (+), respectively (Text S1–S2). Asterisks (*) following the name of *P* dataset indicate
 462 its limited spatial coverage omitting high-latitude regions with typically low performance, and
 463 dashed line in each box indicates median of only 50°S–50°N. * of *SM* dataset indicates that the
 464 dataset does not consider the entire soil column.

465

Deleted: ,



467
468 **Fig. 2. Types of best-performing datasets across hydrological variables.** Colors indicate type
469 of dataset with the highest water balance consistency. Gray color indicates that multiple datasets
470 show similar water balance consistency (with R^2 scores varying by less than 5%) or low water
471 balance consistency (with all R^2 scores below 0.2).

472
473 **3.2 Potential reasons influencing water balance consistency**

474 Next, we aim to diagnose possible reasons for regional discrepancies of dataset performance in
475 terms of water balance consistency. For this purpose, we consider a large set of variables that
476 may affect the water balance consistency of a given dataset, including soil and vegetation
477 characteristics, climate, and gauge density (Methods). By applying an explainable machine
478 learning method (i.e., SHAP), temperature and aridity (i.e., ET/P) were diagnosed as the key
479 factors influencing the spatial performance patterns of the datasets (Fig. 3 and Figs. S17–S20).
480 At the same time, factors like irrigation, urbanization, and lateral flow play relatively minor roles
481 (Figs. S17–S20). For the key factors, our results demonstrate that the performance of P datasets
482 is higher in the sub-humid and sub-arid regions (where the aridity index is 0.6–1.0) with monthly
483 mean temperatures between 10°C and 15°C (Fig. 3a and Fig. S21). The results for ET , R , and SM
484 datasets are largely similar to those of P datasets (Fig. 3b–d and Figs. S22–S24). These influence
485 patterns were summarized according to medians across dataset performance, while using
486 maximum does not alter the results (Fig. S25).

Deleted: varied within

Deleted: lower than

Deleted: to influence

Deleted: P , ET , and R

Deleted: , while for SM datasets temperature and tree cover are critical

Deleted: S16–S19). Our

Deleted: S20

Deleted: R

Deleted: c

Deleted: S21–

Deleted:), while comparatively good performance of SM datasets is found in regions with a moderate tree cover fraction (5–50 %) and warm temperature (10–15 °C) (Fig. 3d and Fig. S23...

Deleted: S24

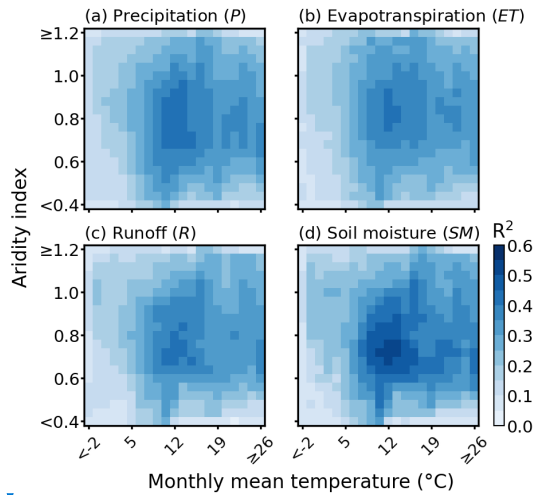
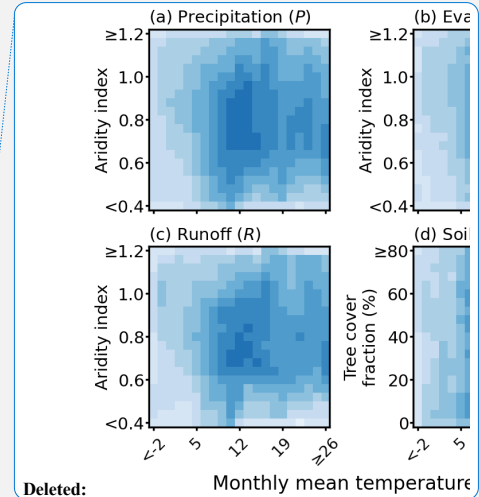


Fig. 3. Influence of temperature and aridity on water balance consistency of datasets. Consistency in water balance is quantified by R^2 scores (Fig. 1), and median R^2 scores across $P/ET/R/SM$ datasets for each climate class are shown (Figs. S21–S24).

3.3 Temporal changes in water balance consistency of dataset

We furthermore assess changes in the diagnosed dataset performance inferred from water balance consistency over time. This is done by splitting our study period and repeating the analysis for the sub-periods 2000–2010 and 2011–2022, and includes an assessment of significance (Methods). For the P datasets, the majority of global grid cells show no temporal change in water balance consistency, and among the grid cells with temporal changes, we found mostly increases (Fig. 4a). These increasing changes were mainly observed in middle- and high-latitude regions of the Northern Hemisphere, while the P dataset from ERA5 shows the highest median level of performance improvement (Fig. S26). At the same time, we find similar spatial patterns of changes in water balance consistency for ET , R , and S datasets, with most grid cells showing no change (Fig. 4b–d). Among the grid cells with significant changes, performance in terms of water balance consistency increases prevail and are mostly located in high-latitude regions and in regions with scarce observations in the Northern Hemisphere (Fig. 4b–d, Fig. S8 and S27–S29).



Deleted: Monthly mean temperature

Deleted: (or tree cover for SM)

Deleted: The consistency through

Deleted: /vegetation

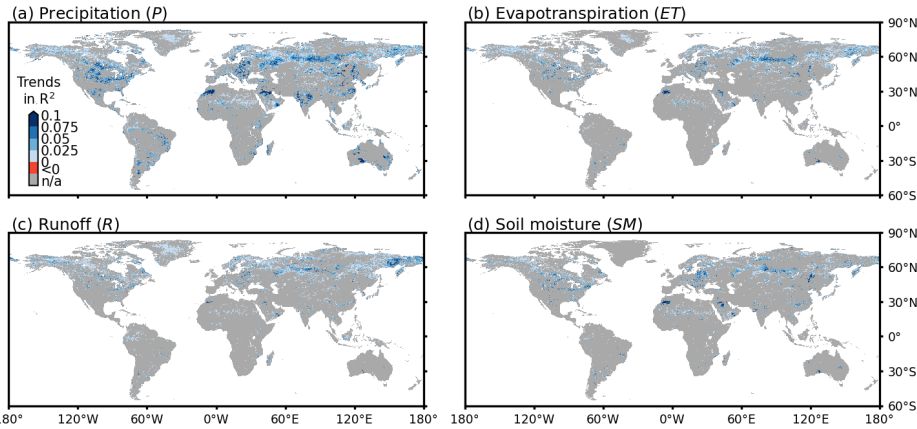
Deleted: (Figs. S20–S23)

Deleted: .

Deleted: S25

Deleted: S14

Deleted: S26–S28



533
534 **Fig. 4. Temporal changes in water balance consistency of P , ET , R , and SM datasets from**
535 **2000–2010 to 2011–2022.** Based on the changes in R scores for each dataset (Figs. S26–S29),
536 median values are shown in each grid cell where at least half the considered datasets showed
537 significant changes (Methods), representing common temporally changing patterns.

538
539 **4 Discussion**

540 The spatial performance patterns derived from our water balance consistency approach reveal
541 high similarity among P datasets (Fig. S4), consistent with findings from recent studies on P
542 dataset agreement (Markonis et al., 2024; Dosio et al., 2021). For the medians of 50°S–50°N,
543 several P datasets like PERSIANN-CDR, GPM IMERG v07, and MSWEP v2.8 are also
544 comparable, which might be related to their close genealogical relationships (Markonis et al.,
545 2024; Vargas Godoy et al., 2025). Beyond these similarities, our grid cell-level comparisons
546 suggest that satellite-based P datasets outperform others in large regions of southern America,
547 Africa, south and Southeast Asia, and inner Australia, while gauge-based P datasets excel in
548 many grid cells across the United States, Europe, and East Asia (Fig. 2). This suggests that the
549 satellite-based P datasets are superior in regions with sparse or no gauging stations (Fig. S8),
550 compared to gauge-based and reanalysis datasets. However, all P datasets exhibit higher water
551 balance consistency in moderately humid or dry regions, with long-term mean temperature also
552 influencing the performance (Fig. 3 and Fig. S21). Lower consistency of gauge-based datasets in
553 humid and dry regions may stem from challenges in mapping spatial variability of extreme
554 rainfall (Mishra and Coulibaly, 2009) and accurately recording light precipitation events (Lanza
555 et al., 2022), as consistency is based on seasonal variabilities in water balance. Additionally, P
556 datasets show lower consistency in cold regions because of difficulties in measuring solid
557 precipitation (La et al., 2002). Similarly, satellite-derived precipitation is relatively insensitive to
558 light rainfall (Laviola et al., 2013), struggles with extreme rainfall estimates (likely due to
559 retrieval algorithms and infrequent temporal sampling of polar orbits) (Barlow et al., 2019), and
560 often fails to detect snowfall or perform well over snow- and ice-covered surfaces (Alijanian et
561 al., 2017). In contrast, reanalysis datasets perform better in cold regions, benefiting from
562 assimilated meteorological observations and atmospheric states (Barlow et al., 2019; Dosio et al.,

Deleted: S25–S28

Deleted: S3

Deleted: 2021).

Deleted: S7

Deleted: S20

2021; Sun et al., 2018).

The *ET*, *R*, and *SM* datasets generally show global spatial performance patterns similar to those of *P* datasets (Figs. S4–S7). This is partly because uncertainties in *P* datasets propagate through the water cycle (Fallah et al., 2020), affecting the water of the water balances of *ET*, *R*, and *SM* datasets. Limitations in representing snowpack and permafrost processes, along with difficulties in satellite retrievals over snow- and ice-covered high-latitude regions, also contribute to this issue (Hirschi et al., 2025; Muñoz-Sabater et al., 2021). Nevertheless, our approach identifies distinct relative performances across hydrological variables and dataset types (Fig. 2 and Fig. S16), as it considers independent combinations of datasets. For *ET*, the satellite-based PT-JPL dataset performs comparatively well, likely due to its advanced consideration of plant physiological limitations and water stress. The reanalysis dataset GLDAS-2.2 also performs comparatively well, probably due to its assimilation of terrestrial water storage (Table S2 and Fig. S16). For *R*, the machine-learning model-driven GRUN, constrained by *P* and temperature in large basins, and ERA5-land dataset, perform best in most regions (Tables S3 and Fig. S16). For *SM*, reanalysis datasets perform best, likely because they are constrained by physical laws and consider deeper soil moisture variability (Table S4 and Fig. S16). In contrast, low penetration depths (~2–5 cm) of microwave sensors limit the ability of ESA CCI v08.1 to capture deeper-layer *SM* variations (Hirschi et al., 2025). Overall, our results highlight the importance of physical constraints and of data assimilation in enhancing water balance consistency of hydrological variables (Pan et al., 2020; Tang et al., 2024; Yang et al., 2023; Ruiz-Vásquez et al., 2023).

Dataset performance varied significantly across time scales, with the highest correspondence at the monthly scale, where seasonal variability is well-captured and synoptic weather variability is mitigated. This explains the markedly lower water balance consistency observed at the annual scale for all datasets, where seasonal signals are strongly smoothed. At a daily time scale, the variability of the involved variables is high, including more extreme values and high noise, and apparently under-constrained by available observations (Maurer and Hidalgo, 2008; Fisher et al., 2008). Furthermore, we find widespread increases in water balance consistency across hydrological variables during our study period in mid-to-high latitude regions of the Northern Hemisphere (Fig. 4). These regions have experienced reduced snow-cover durations (Bormann et al., 2018) and extents (Mudryk et al., 2020), as well as less snowfall (O’Gorman, 2014), which has weakened *R* seasonality (Wang et al., 2024) and enhanced the influence of *P* variability on *R* seasonality (Han et al., 2024). Given the influence patterns in Fig. 3, higher temperatures and reduced solid precipitation likely enhance *P* dataset performance. Also, the absence of strong increases in extreme precipitation events in these regions (Asadieh and Krakauer, 2015) may contribute to improved consistency. Previous studies have shown that models incorporating updated vegetation information, such as leaf area index (LAI) seasonality, perform better in these regions (Ruiz-Vásquez et al., 2023; Nogueira et al., 2021), aligning with our observed improvements over time (Fig. 4). This indicates the role of vegetation characteristics in accurately representing the coupling between *ET* and *SM* for dataset performance, as inferred from our approach.

Data availability

All data needed to evaluate the conclusions in the paper are present in the paper and/or the online

Deleted: S6

Deleted: balance consistency of *ET*, *R*, and *SM* datasets.

Deleted: S14

Deleted: S14

Deleted: S14

Deleted: considers

Deleted: S14

Formatted

Deleted: extremely

Deleted: O’gorman

Deleted: underscores

Deleted: importance

623 repository. Additionally, their access links are provided in the following. CPC is available at
624 <https://www.psl.noaa.gov/data/gridded/data.cpc.globalprecip.html>; CRU TS v4.06 is available at
625 https://crudata.uea.ac.uk/cru/data/hrg/cru_ts_4.06/; UDel v5.01 is available at
626 <https://climate.geog.udel.edu/>; EM-EARTH is available at [https://www.frdr-](https://www.frdr-dfdr.ca/repo/dataset/8d30ab02-f2bd-4d05-ae43-11f4a387e5ad)
627 [dfdr.ca/repo/dataset/8d30ab02-f2bd-4d05-ae43-11f4a387e5ad](https://www.frdr-dfdr.ca/repo/dataset/8d30ab02-f2bd-4d05-ae43-11f4a387e5ad); GPCC v2022 is available at
628 [https://opendata.dwd.de/climate_environment/GPCC/html/fulldata-](https://opendata.dwd.de/climate_environment/GPCC/html/fulldata-monthly_v2022_doi_download.html)
629 [monthly_v2022_doi_download.html](https://opendata.dwd.de/climate_environment/GPCC/html/fulldata-monthly_v2022_doi_download.html); PREC/L is available at
630 <https://psl.noaa.gov/data/gridded/data.precl.html>; CHIRPS v2.0 is available at
631 <https://www.chc.ucsb.edu/data/chirps>; CMAP is available at
632 <https://psl.noaa.gov/data/gridded/data.cmap.html>; CMORPH v1 is available at
633 <https://www.ncei.noaa.gov/products/climate-data-records/precipitation-cmorph>; GPCP(M) v2.3
634 is available at <https://psl.noaa.gov/data/gridded/data.gpcp.html>; GPCP(D) v1.3 is available at
635 <https://rda.ucar.edu/datasets/d728007/>; GPM IMERG v07 is available at
636 [https://disc.gsfc.nasa.gov/datasets/GPM_3IMERGDF_07/summary?keywords=%22IMERG%20](https://disc.gsfc.nasa.gov/datasets/GPM_3IMERGDF_07/summary?keywords=%22IMERG%20final%22)
637 [final%22](https://disc.gsfc.nasa.gov/datasets/GPM_3IMERGDF_07/summary?keywords=%22IMERG%20final%22); PERSIANN-CDR is available at [https://www.ncei.noaa.gov/products/climate-data-](https://www.ncei.noaa.gov/products/climate-data-records/precipitation-persiann)
638 [records/precipitation-persiann](https://www.ncei.noaa.gov/products/climate-data-records/precipitation-persiann); MSWEP v2.8 is available at <https://www.gloh2o.org/mswep/>;
639 20CR v3 is available at https://psl.noaa.gov/data/gridded/data.20thC_ReanV3.html; JRA-55 is
640 available at <https://rda.ucar.edu/datasets/d628000/>; ERA5 is available at
641 <https://cds.climate.copernicus.eu/datasets/reanalysis-era5-single-levels?tab=overview>; NCEP-
642 NCAR R1 is available at <https://psl.noaa.gov/data/gridded/data.ncep.reanalysis.html>; NCEP-
643 DOE R2 is available at <https://psl.noaa.gov/data/gridded/data.ncep.reanalysis2.html>; MERRA-2
644 is available at https://gmao.gsfc.nasa.gov/reanalysis/MERRA-2/data_access/; X-BASE is
645 available at https://meta.icos-cp.eu/collections/_185vWiIV81AifoxCkty50YI; MODIS is
646 available at <https://lpdaac.usgs.gov/products/mod16a2gfv061/>; PT-JPL is available at
647 <http://josh.yosh.org/>; PML-v2 is available at <https://doi.org/10.5281/zenodo.10647618> (Zhang et
648 al., 2024b); GLASS is available at <http://www.glass.umd.edu/Download.html>; GLEAM v4.1 is
649 available at <https://www.gleam.eu/>; GLDAS-2.0/2.1/2.2 are available at
650 <https://disc.gsfc.nasa.gov/datasets?keywords=GLDAS>; ERA5-land is available at
651 <https://cds.climate.copernicus.eu/datasets/reanalysis-era5-land?tab=overview>; GRUN is available
652 at https://figshare.com/articles/dataset/GRUN_Global_Runoff_Reconstruction/9228176; SMAP
653 L4 v7 is available at <https://nsidc.org/data/spl4smgp/versions/7>; SoMo.ml is available at
654 <https://www.bgc-jena.mpg.de/geodb/projects/Data.php>; ESA CCI v08.1 is available at
655 <https://climate.esa.int/en/projects/soil-moisture/>.

656

657 **Code availability**

658 The core codes for calculating the water balance consistency of each combination and each
659 dataset, as well as assessing the potential influence based on explainable machine learning and
660 uncertainties of the temporal changes based on bootstrap confidence intervals, are available at
661 <https://github.com/HowHuang/WaterBalanceConsistency>.

662

663 **Author contributions**

664 R.O. conceived the original idea, which was further developed in collaboration with H.H. and
665 J.L. H.H. aggregated the datasets used in this study, did the analysis, and prepared the original
666 paper. H.H., J.L., A.C., M.R.V., and R.O. contributed to interpreting the results and discussion

667 and improving the paper.

668

669 **Competing interests**

670 The authors declare that they have no competing interests.

671

672 **Acknowledgments**

673 We thank the respective dataset development groups for their continuous efforts in advancing the
674 state-of-the-art datasets and ensuring easy access. We furthermore thank Sophia Walther (Max
675 Planck Institute for Biogeochemistry, Jena), as well as the Biogeochemical System Modeling,
676 Biometry and Environmental System Analysis (led by Carsten F. Dormann), and Sensor-based
677 Geoinformatics (led by Teja Kattenborn) groups at the University of Freiburg, for fruitful
678 discussions.

679

680 **Competing interests**

681 The authors declare no competing interests.

682

683 **Financial support**

684 J.L. acknowledges support from the National Natural Science Foundation of China (Grant No.
685 42361144001), the 111 Project (Grant No. D25014), the National Foreign Experts Program
686 (Category S) (Grant No. S20240116), and the Henan Province Foreign Scientist Studio for
687 Synergistic Management of Water, Food, Energy, and Carbon (Grant No. GZS2024013). A.C.
688 acknowledges support from Guangdong Provincial Key Laboratory of Intelligent Disaster
689 Prevention and Emergency Technologies for Urban Lifeline Engineering (2022) (Grant No.
690 2022B1212010016). H.H. acknowledges a scholarship from the China Scholarship Council for
691 visiting the University of Freiburg to complete this study and work with many cool scientists.
692 R.O. acknowledges support from the German Research Foundation (Emmy Noether Grant No.
693 391059971).

694

695 **References**

696 Abolafia-Rosenzweig, R., Pan, M., Zeng, J. L., and Livneh, B.: Remotely sensed ensembles of
 697 the terrestrial water budget over major global river basins: An assessment of three closure
 698 techniques, *Remote Sensing of Environment*, 252, <https://doi.org/10.1016/j.rse.2020.112191>,
 699 2021.

700 Adler, R. F., Sapiiano, M., Huffman, G. J., Wang, J., Gu, G., Bolvin, D., Chiu, L., Schneider, U.,
 701 Becker, A., Nelkin, E., Xie, P., Ferraro, R., and Shin, D. B.: The Global Precipitation
 702 Climatology Project (GPCP) Monthly Analysis (New Version 2.3) and a Review of 2017
 703 Global Precipitation, *Atmosphere*, 9, <https://doi.org/10.3390/atmos9040138>, 2018.

704 Alijanian, M., Rakhshandehroo, G. R., Mishra, A. K., and Dehghani, M.: Evaluation of satellite
 705 rainfall climatology using CMORPH, PERSIANN-CDR, PERSIANN, TRMM, MSWEP over
 706 Iran, *International Journal of Climatology*, 37, 4896-4914, <https://doi.org/10.1002/joc.5131>,
 707 2017.

708 Asadieh, B. and Krakauer, N. Y.: Global trends in extreme precipitation: climate models versus
 709 observations, *Hydrology and Earth System Sciences*, 19, 877-891,
 710 <https://doi.org/10.5194/hess-19-877-2015>, 2015.

711 Ashouri, H., Hsu, K. L., Sorooshian, S., Braithwaite, D. K., Knapp, K. R., Cecil, L. D., Nelson,
 712 B. R., and Prat, O. P.: PERSIANN-CDR Daily Precipitation Climate Data Record from
 713 Multisatellite Observations for Hydrological and Climate Studies, *Bulletin of the American
 714 Meteorological Society*, 96, 69-83, <https://doi.org/10.1175/Bams-D-13-00068.1>, 2015.

715 Barlow, M., Gutowski, W. J., Gyakum, J. R., Katz, R. W., Lim, Y.-K., Schumacher, R. S.,
 716 Wehner, M. F., Agel, L., Bosilovich, M., Collow, A., Gershunov, A., Grotjahn, R., Leung, R.,
 717 Milrad, S., and Min, S.-K.: North American extreme precipitation events and related large-
 718 scale meteorological patterns: a review of statistical methods, dynamics, modeling, and
 719 trends, *Climate Dynamics*, 53, 6835-6875, <https://doi.org/10.1007/s00382-019-04958-z>, 2019.

720 Beck, H. E., Wood, E. F., Pan, M., Fisher, C. K., Miralles, D. G., van Dijk, A. I. J. M., McVicar,
 721 T. R., and Adler, R. F.: MSWEP V2 Global 3-Hourly 0.1 degrees Precipitation: Methodology
 722 and Quantitative Assessment, *Bulletin of the American Meteorological Society*, 100, 473-502,
 723 <https://doi.org/10.1175/Bams-D-17-0138.1>, 2019.

724 Bormann, K. J., Brown, R. D., Derksen, C., and Painter, T. H.: Estimating snow-cover trends
 725 from space, *Nature Climate Change*, 8, 923-927, <https://doi.org/10.1038/s41558-018-0318-3>,
 726 2018.

727 Chen, M. Y., Xie, P. P., Janowiak, J. E., and Arkin, P. A.: Global land precipitation: A 50-yr
 728 monthly analysis based on gauge observations, *Journal of Hydrometeorology*, 3, 249-266,
 729 [https://doi.org/10.1175/1525-7541\(2002\)003<0249:GLPAYM>2.0.CO;2](https://doi.org/10.1175/1525-7541(2002)003<0249:GLPAYM>2.0.CO;2), 2002.

730 Cleophas, F., Isidore, F., Musta, B., Mohd Ali, B. N., Mahali, M., Zahari, N. Z., and Bidin, K.:
 731 Effect of soil physical properties on soil infiltration rates, *Journal of Physics: Conference
 732 Series*, 2314, <https://doi.org/10.1088/1742-6596/2314/1/012020>, 2022.

733 Denissen, J. M. C., Teuling, A. J., Pitman, A. J., Koirala, S., Migliavacca, M., Li, W. T.,
 734 Reichstein, M., Winkler, A. J., Zhan, C. H., and Orth, R.: Widespread shift from ecosystem
 735 energy to water limitation with climate change, *Nature Climate Change*, 12, 677-684,
 736 <https://doi.org/10.1038/s41558-022-01403-8>, 2022.

737 Do, H. X., Gudmundsson, L., Leonard, M., and Westra, S.: The Global Streamflow Indices and
 738 Metadata Archive (GSIM) - Part 1: The production of a daily streamflow archive and
 739 metadata, *Earth System Science Data*, 10, 765-785, <https://doi.org/10.5194/essd-10-765-2018>,
 740 2018.

Formatted: Font: Italic

Deleted: (Basel),

Formatted: Font: Italic

Formatted: Font: Italic

Formatted: Font: Italic

Formatted: Font: Italic

Deleted: -+,

Formatted: Font: Italic

Formatted: Font: Italic

Formatted: Font: Italic

Formatted: Font: Italic

Deleted: Doi

Deleted: Glpaym

Deleted: Co

Formatted: Font: Italic

Moved down [1]: . B.,

Deleted: Cooley, S. S., Fisher, J

Deleted: and Goldsmith, G. R.: Convergence in water use efficiency within plant functional types across contrasting climates, *Nat Plants*, 8, 341-345, [10.1038/s41477-022-01131-z](https://doi.org/10.1038/s41477-022-01131-z), 2022.

Formatted: Font: Italic

Formatted: Font: Italic

752 [Dorigo, W., Himmelbauer, I., Aberer, D., Schremmer, L., Petrakovic, I., Zappa, L.,](#)
753 [Preimesberger, W., Xaver, A., Annor, F., Ardö, J., Baldocchi, D., Bitelli, M., Blöschl, G.,](#)
754 [Bogena, H., Brocca, L., Calvet, J. C., Camarero, J. J., Capello, G., Choi, M., Cosh, M. C., van](#)
755 [de Giesen, N., Hajdu, I., Ikonen, J., Jensen, K. H., Kanniah, K. D., de Kat, I., Kirchengast, G.,](#)
756 [Rai, P. K., Kyrouac, J., Larson, K., Liu, S. X., Loew, A., Moghaddam, M., Fernández, J. M.,](#)
757 [Bader, C. M., Morbidelli, R., Musial, J. P., Osenga, E., Palecki, M. A., Pellarin, T.,](#)
758 [Petropoulos, G. P., Pfiel, I., Powers, J., Robock, A., Rüdiger, C., Rummel, U., Strobel, M., Su,](#)
759 [Z. B., Sullivan, R., Tagesson, T., Varlagin, A., Vreugdenhil, M., Walker, J., Wen, J., Wenger,](#)
760 [F., Wigneron, J. P., Woods, M., Yang, K., Zeng, Y. J., Zhang, X., Zreda, M., Dietrich, S.,](#)
761 [Gruber, A., van Oevelen, P., Wagner, W., Scipal, K., Drusch, M., and Sabia, R.: The](#)
762 [International Soil Moisture Network: serving Earth system science for over a decade,](#)
763 [Hydrology and Earth System Sciences, 25, 5749-5804, \[https://doi.org/10.5194/hess-25-5749-\]\(https://doi.org/10.5194/hess-25-5749-2021\)](#)
764 [2021, 2021.](#)

765 [Dormann, C. F., Elith, J., Bacher, S., Buchmann, C., Carl, G., Carré, G., Marquéz, J. R. G.,](#)
766 [Gruber, B., Lafourcade, B., Leitão, P. J., Münkemüller, T., McClean, C., Osborne, P. E.,](#)
767 [Reineking, B., Schröder, B., Skidmore, A. K., Zurell, D., and Lautenbach, S.: Collinearity: a](#)
768 [review of methods to deal with it and a simulation study evaluating their performance,](#)
769 [Ecography, 36, 27-46, <https://doi.org/10.1111/j.1600-0587.2012.07348.x>, 2012.](#)

770 [Dosio, A., Pinto, I., Lennard, C., Sylla, M. B., Jack, C., and Nikulin, G.: What can we know](#)
771 [about recent past precipitation over Africa? Daily characteristics of African precipitation from](#)
772 [a large ensemble of observational products for model evaluation, Earth and Space Science, 8,](#)
773 [https://doi.org/10.1029/2020EA001466, 2021.](#)

774 [Douville, H., Raghavan, K., Renwick, J., Allan, R. P., Arias, P. A., Barlow, M., Cerezo-Mota, R.,](#)
775 [Cherchi, A., Gan, T., and Gergis, J.: Water cycle changes, Climate change 2021: The physical](#)
776 [science basis. Contribution of working group I to 45 the sixth assessment report of the](#)
777 [intergovernmental panel on climate change, 1055-1210, 2021.](#)

778 [Fallah, A., O, S., and Orth, R.: Climate-dependent propagation of precipitation uncertainty into](#)
779 [the water cycle, Hydrology and Earth System Sciences, 24, 3725-3735,](#)
780 [https://doi.org/10.5194/hess-24-3725-2020, 2020.](#)

781 [Fisher, J. B., Tu, K. P., and Baldocchi, D. D.: Global estimates of the land-atmosphere water flux](#)
782 [based on monthly AVHRR and ISLSCP-II data, validated at 16 FLUXNET sites, Remote](#)
783 [Sensing of Environment, 112, 901-919, <https://doi.org/10.1016/j.rse.2007.06.025>, 2008.](#)

784 [Freedman, F. R., Pitts, K. L., and Bridger, A. F. C.: Evaluation of CMIP climate model](#)
785 [hydrological output for the Mississippi River Basin using GRACE satellite observations,](#)
786 [Journal of Hydrology, 519, 3566-3577, <https://doi.org/10.1016/j.jhydrol.2014.10.036>, 2014.](#)

787 [Funk, C., Peterson, P., Landsfeld, M., Pedreros, D., Verdin, J., Shukla, S., Husak, G., Rowland,](#)
788 [J., Harrison, L., Hoell, A., and Michaelsen, J.: The climate hazards infrared precipitation with](#)
789 [stations-a new environmental record for monitoring extremes, Scientific Data, 2,](#)
790 [https://doi.org/10.1038/sdata.2015.66, 2015.](#)

791 [Gebrechorkos, S. H., Leyland, J., Dadson, S. J., Cohen, S., Slater, L., Wortmann, M., Ashworth,](#)
792 [P. J., Bennett, G. L., Boothroyd, R., Cloke, H., Delorme, P., Griffith, H., Hardy, R., Hawker,](#)
793 [L., McLelland, S., Neal, J., Nicholas, A., Tatem, A. J., Vahidi, E., Liu, Y. X., Sheffield, J.,](#)
794 [Parsons, D. R., and Darby, S. E.: Global-scale evaluation of precipitation datasets for](#)
795 [hydrological modelling, Hydrology and Earth System Sciences, 28, 3099-3118,](#)
796 [https://doi.org/10.5194/hess-28-3099-2024, 2024.](#)

797 [Gelaro, R., McCarty, W., Suarez, M. J., Todling, R., Molod, A., Takacs, L., Randles, C.,](#)

Moved (insertion) [2]

Moved (insertion) [3]

Moved (insertion) [4]

Moved (insertion) [1]

Moved (insertion) [5]

Deleted: Dorigo, W. A., Wagner, W., Hohensinn, R., Hahn, S., Paulik,

Moved up [3]: C., Xaver, A.,

Moved up [2]: Xaver, A.,

Moved up [4]: A.,

Moved up [5]: ., van Oevelen, P.,

Deleted: Gruber,

Deleted: Drusch, M., Mecklenburg, S

Deleted: Robock, A., and Jackson, T.: The International Soil Moisture Network: a data hosting facility for global in situ soil moisture measurements, Hydrology and Earth System Sciences, 15, 1675-1698, 10.5194/hess-15-1675-2011, 2011.

Formatted: Font: Italic

Formatted: Font: Italic

Deleted: 2021.

Formatted: Font: Italic

Formatted: Font: Italic

Formatted: Font: Italic

Formatted: Font: Italic

Formatted: Font: Italic

811 Darnenov, A., Bosilovich, M. G., Reichle, R., Wargan, K., Coy, L., Cullather, R., Draper, C.,
812 Akella, S., Buchard, V., Conaty, A., da Silva, A., Gu, W., Kim, G. K., Koster, R., Lucchesi, R.,
813 Merkova, D., Nielsen, J. E., Partyka, G., Pawson, S., Putman, W., Rienecker, M., Schubert, S.
814 D., Sienkiewicz, M., and Zhao, B.: The Modern-Era Retrospective Analysis for Research and
815 Applications, Version 2 (MERRA-2), *Journal of Climate*, 30, 5419-5454,
816 <https://doi.org/10.1175/JCLI-D-16-0758.1>, 2017.

817 Ghiggi, G., Humphrey, V., Seneviratne, S. I., and Gudmundsson, L.: GRUN: an observation-
818 based global gridded runoff dataset from 1902 to 2014, *Earth System Science Data*, 11, 1655-
819 1674, <https://doi.org/10.5194/essd-11-1655-2019>, 2019.

820 Gong, P., Li, X. C., Wang, J., Bai, Y. Q., Cheng, B., Hu, T. Y., Liu, X. P., Xu, B., Yang, J., Zhang,
821 W., and Zhou, Y. Y.: Annual maps of global artificial impervious area (GAIA) between 1985
822 and 2018, *Remote Sensing of Environment*, 236, <https://doi.org/10.1016/j.rse.2019.111510>,
823 2020.

824 Greve, P., Orlowsky, B., Mueller, B., Sheffield, J., Reichstein, M., and Seneviratne, S. I.: Global
825 assessment of trends in wetting and drying over land, *Nature Geoscience*, 7, 716-721,
826 <https://doi.org/10.1038/ngeo2247>, 2014.

827 Gruber, A., Scanlon, T., van der Schalie, R., Wagner, W., and Dorigo, W.: Evolution of the ESA
828 CCI Soil Moisture climate data records and their underlying merging methodology, *Earth
829 System Science Data*, 11, 717-739, <https://doi.org/10.5194/essd-11-717-2019>, 2019.

830 Han, J., Liu, Z., Woods, R., McVicar, T. R., Yang, D., Wang, T., Hou, Y., Guo, Y., Li, C., and
831 Yang, Y.: Streamflow seasonality in a snow-dwindling world, *Nature*, 629, 1075-1081,
832 <https://doi.org/10.1038/s41586-024-07299-y>, 2024.

833 Hansen, M. and Song, X.: Vegetation Continuous Fields (VCF) Yearly Global 0.05 Deg,
834 <https://doi.org/10.5067/MEaSURES/VCF/VCF5KYR.001>, 2018.

835 Harris, I., Osborn, T. J., Jones, P., and Lister, D.: Version 4 of the CRU TS monthly high-
836 resolution gridded multivariate climate dataset, *Scientific Data*, 7, 109,
837 <https://doi.org/10.1038/s41597-020-0453-3>, 2020.

838 Hersbach, H., Bell, B., Berrisford, P., Hirahara, S., Horányi, A., Muñoz-Sabater, J., Nicolas, J.,
839 Peubey, C., Radu, R., Schepers, D., Simmons, A., Soci, C., Abdalla, S., Abellan, X., Balsamo,
840 G., Bechtold, P., Biavati, G., Bidlot, J., Bonavita, M., De Chiara, G., Dahlgren, P., Dee, D.,
841 Diamantakis, M., Dragani, R., Flemming, J., Forbes, R., Fuentes, M., Geer, A., Haimberger,
842 L., Healy, S., Hogan, R. J., Hólm, E., Janisková, M., Keeley, S., Laloyaux, P., Lopez, P., Lupu,
843 C., Radnoti, G., de Rosnay, P., Rozum, I., Vamborg, F., Villaume, S., and Thépaut, J. N.: The
844 ERA5 global reanalysis, *Quarterly Journal of the Royal Meteorological Society*, 146, 1999-
845 2049, <https://doi.org/10.1002/qj.3803>, 2020.

846 Hirschi, M., Stradiotti, P., Crezee, B., Dorigo, W., and Seneviratne, S. I.: Potential of long-term
847 satellite observations and reanalysis products for characterising soil drying: trends and
848 drought events, *Hydrology and Earth System Sciences*, 29, 397-425,
849 <https://doi.org/10.5194/hess-29-397-2025>, 2025.

850 Huffman, G. J., Stocker, E. F., Bolvin, D. T., Nelkin, E. J., and Tan, J.: GPM IMERG Final
851 Precipitation L3 1 day 0.1 degree x 0.1 degree V07,
852 <https://doi.org/10.5067/GPM/IMERGDF/DAY/07>, 2023.

853 Huffman, G. J., Adler, R. F., Morrissey, M. M., Bolvin, D. T., Curtis, S., Joyce, R., McGavock,
854 B., and Susskind, J.: Global precipitation at one-degree daily resolution from multisatellite
855 observations, *Journal of Hydrometeorology*, 2, 36-50, [https://doi.org/10.1175/1525-7541\(2001\)002<0036:Gpaodd>2.0.Co;2](https://doi.org/10.1175/1525-7541(2001)002<0036:Gpaodd>2.0.Co;2), 2001.

Deleted: Volume

Formatted: Font: Italic

Formatted: Font: Italic

Formatted: Font: Italic

Formatted: Font: Italic

Formatted: Font: Italic

Formatted: Font: Italic

Deleted: Q J Roy Meteor Soc

Formatted: Font: Italic

Deleted: Doi

Formatted: Font: Italic

860 Japan Meteorological Agency, J.: JRA-55: Japanese 55-year Reanalysis, Monthly Means and
861 Variances, <https://doi.org/10.5065/D60G3H5B>, 2013.

862 Jaramillo, F. and Destouni, G.: Local flow regulation and irrigation raise global human water
863 consumption and footprint, *Science*, 350, 1248-1251, <https://doi.org/10.1126/science.aad1010>,
864 2015.

865 Kanamitsu, M., Ebisuzaki, W., Woollen, J., Yang, S. K., Hnilo, J. J., Fiorino, M., and Potter, G.
866 L.: NCEP-DOE AMIP-II reanalysis (R-2), *Bulletin of the American Meteorological Society*,
867 83, 1631-1643, [https://doi.org/10.1175/Bams-83-11-1631\(2002\)083<1631:Nar>2.3.Co;2](https://doi.org/10.1175/Bams-83-11-1631(2002)083<1631:Nar>2.3.Co;2),
868 2002.

869 Kistler, R., Kalnay, E., Collins, W., Saha, S., White, G., Woollen, J., Chelliah, M., Ebisuzaki, W.,
870 Kanamitsu, M., Kousky, V., van den Dool, H., Jenne, R., and Fiorino, M.: The NCEP-NCAR
871 50-year reanalysis: Monthly means CD-ROM and documentation, *Bulletin of the American*
872 *Meteorological Society*, 82, 247-267, [https://doi.org/10.1175/1520-0477\(2001\)082<0247:Tnnyrm>2.3.Co;2](https://doi.org/10.1175/1520-0477(2001)082<0247:Tnnyrm>2.3.Co;2), 2001.

873 Kulesa, A., Krzywinski, M., Blainey, P., and Altman, N.: Sampling distributions and the
874 bootstrap, *Nature Methods*, 12, 477-478, <https://doi.org/10.1038/nmeth.3414>, 2015.

875 La Barbera, P., Lanza, L., and Stagi, L.: Tipping bucket mechanical errors and their influence on
876 rainfall statistics and extremes, *Water Science and Technology*, 45, 1-9, 2002.

877 Lanza, L. G., Cauteruccio, A., and Stagnaro, M.: Rain gauge measurements, in: *Rainfall*,
878 Elsevier, 77-108, 2022.

879 Laviola, S., Levizzani, V., Cattani, E., and Kidd, C.: The 183-WSL fast rain rate retrieval
880 algorithm. Part II: Validation using ground radar measurements, *Atmospheric Research*, 134,
881 77-86, <https://doi.org/10.1016/j.atmosres.2013.07.013>, 2013.

882 Legates, D. R. and Willmott, C. J.: Mean seasonal and spatial variability in gauge-corrected,
883 global precipitation, *International Journal of Climatology*, 10, 111-127,
884 <https://doi.org/10.1002/joc.3370100202>, 1990.

885 Li, B., Rodell, M., Sheffield, J., Wood, E., and Sutanudjaja, E.: Long-term, non-anthropogenic
886 groundwater storage changes simulated by three global-scale hydrological models, *Scientific*
887 *Reports*, 9, 10746, <https://doi.org/10.1038/s41598-019-47219-z>, 2019.

888 Li, W., Migliavacca, M., Forkel, M., Denissen, J. M. C., Reichstein, M., Yang, H., Duveiller, G.,
889 Weber, U., and Orth, R.: Widespread increasing vegetation sensitivity to soil moisture, *Nature*
890 *Communications*, 13, 3959, <https://doi.org/10.1038/s41467-022-31667-9>, 2022.

891 Li, W., Reichstein, M., O, S., May, C., Destouni, G., Migliavacca, M., Kraft, B., Weber, U., and
892 Orth, R.: Contrasting Drought Propagation Into the Terrestrial Water Cycle Between Dry and
893 Wet Regions, *Earth's Future*, 11, e2022EF003441, <https://doi.org/10.1029/2022ef003441>,
894 2023a.

895 Li, W., Pacheco-Labrador, J., Migliavacca, M., Miralles, D., Hoek van Dijke, A., Reichstein, M.,
896 Forkel, M., Zhang, W., Frankenberg, C., Panwar, A., Zhang, Q., Weber, U., Gentine, P., and
897 Orth, R.: Widespread and complex drought effects on vegetation physiology inferred from
898 space, *Nature Communications*, 14, 4640, <https://doi.org/10.1038/s41467-023-40226-9>,
899 2023b.

900 Markonis, Y., Godoy, M. R. V., Pradhan, R. K., Pratap, S., Thomson, J. R., Hanel, M., Paschalis,
901 A., Nikolopoulos, E., and Papalexiou, S. M.: Spatial partitioning of terrestrial precipitation
902 reveals varying dataset agreement across different environments, *Communications Earth &*
903 *Environment*, 5, <https://doi.org/10.1038/s43247-024-01377-9>, 2024.

904 Maurer, E. P. and Hidalgo, H. G.: Utility of daily vs. monthly large-scale climate data: an

Deleted:

Formatted: Font: Italic

Formatted: Font: Italic

Formatted: Font: Italic

Deleted: Nat

Formatted: Font: Italic

Deleted: , B.

Deleted: . G

Deleted: Sci Technol

Deleted: 10

Formatted: Font: Italic

Formatted: Font: Italic

Deleted: Atmos Res

Deleted: -

Formatted: Font: Italic

Deleted: Sci Rep

Formatted: Font: Italic

Formatted: Font: Italic

Deleted: Nat Commun

Formatted: Font: Italic

916 intercomparison of two statistical downscaling methods, *Hydrology and Earth System*
917 *Sciences*, 12, 551-563, <https://doi.org/10.5194/hess-12-551-2008>, 2008.

918 McCabe, M. F., Rodell, M., Alsdorf, D. E., Miralles, D. G., Uijlenhoet, R., Wagner, W., Lucieer,
919 A., Houborg, R., Verhoest, N. E. C., Franz, T. E., Shi, J., Gao, H., and Wood, E. F.: The Future
920 of Earth Observation in Hydrology, *Hydrology and Earth System Sciences*, 21, 3879-3914,
921 <https://doi.org/10.5194/hess-21-3879-2017>, 2017.

922 Mehta, P., Siebert, S., Kummu, M., Deng, Q., Ali, T., Marston, L., Xie, W., and Davis, K. F.: Half
923 of twenty-first century global irrigation expansion has been in water-stressed regions, *Nature*
924 *Water*, 2, 254-261, <https://doi.org/10.1038/s44221-024-00206-9>, 2024.

925 Mekonnen, M. M. and Hoekstra, A. Y.: Four billion people facing severe water scarcity, *Science*
926 *Advance*, 2, e1500323, <https://doi.org/10.1126/sciadv.1500323>, 2016.

927 Miguez-Macho, G. and Fan, Y.: A global humidity index with lateral hydrologic flows, *Nature*,
928 644, 413-419, <https://doi.org/10.1038/s41586-025-09359-3>, 2025.

929 Miralles, D. G., Bonte, O., Koppa, A., Baez-Villanueva, O. M., Tronquo, E., Zhong, F., Beck, H.
930 E., Hulsman, P., Dorigo, W., Verhoest, N. E. C., and Haghdoust, S.: GLEAM4: global land
931 evaporation and soil moisture dataset at 0.1 resolution from 1980 to near present, *Scientific*
932 *Data*, 12, 416, <https://doi.org/10.1038/s41597-025-04610-y>, 2025.

933 Mishra, A. K. and Coulbaly, P.: Developments in hydrometric network design: A review,
934 *Reviews of Geophysics*, 47, <https://doi.org/10.1029/2007rg000243>, 2009.

935 Mudryk, L., Santolaria-Otín, M., Krinner, G., Ménégoz, M., Derksen, C., Brutel-Vuilmet, C.,
936 Brady, M., and Essery, R.: Historical Northern Hemisphere snow cover trends and projected
937 changes in the CMIP6 multi-model ensemble, *Cryosphere*, 14, 2495-2514,
938 <https://doi.org/10.5194/tc-14-2495-2020>, 2020.

939 Muñoz-Sabater, J., Dutra, E., Agustí-Panareda, A., Albergel, C., Arduini, G., Balsamo, G.,
940 Boussetta, S., Choulga, M., Harrigan, S., Hersbach, H., Martens, B., Miralles, D. G., Piles,
941 M., Rodríguez-Fernández, N. J., Zsoter, E., Buontempo, C., and Thépaut, J.-N.: ERA5-Land:
942 a state-of-the-art global reanalysis dataset for land applications, *Earth System Science Data*,
943 13, 4349-4383, <https://doi.org/10.5194/essd-13-4349-2021>, 2021.

944 Nachtergaele, F., van Velthuizen, H., Verelst, L., Wiberg, D., Henry, M., Chiozza, F., Yigini, Y.,
945 Aksoy, E., Batjes, N., and Boateng, E.: Harmonized world soil database version 2.0, *FAO*,
946 2023.

947 Nelson, J. A., Walther, S., Gans, F., Kraft, B., Weber, U., Novick, K., Buchmann, N.,
948 Migliavacca, M., Wohlfahrt, G., Šigut, L., Ibrom, A., Papale, D., Göckede, M., Duveiller, G.,
949 Knohl, A., Hörtnagl, L., Scott, R. L., Zhang, W., Hamdi, Z. M., Reichstein, M., Aranda-
950 Barranco, S., Ardö, J., Op de Beeck, M., Billesbach, D., Bowling, D., Bracho, R., Brümmer,
951 C., Camps-Valls, G., Chen, S., Cleverly, J. R., Desai, A., Dong, G., El-Madany, T. S.,
952 Euskirchen, E. S., Feigenwinter, I., Galvagno, M., Gerosa, G. A., Gielen, B., Goded, I.,
953 Goslee, S., Gough, C. M., Heinesch, B., Ichii, K., Jackowicz-Korczynski, M. A.,
954 Klosterhalfen, A., Knox, S., Kobayashi, H., Kohonen, K.-M., Korciakoski, M., Mammarella,
955 I., Gharun, M., Marzuoli, R., Matamala, R., Metzger, S., Montagnani, L., Nicolini, G.,
956 O'Halloran, T., Ourcival, J.-M., Peichl, M., Pendall, E., Ruiz Reverter, B., Roland, M.,
957 Sabbatini, S., Sachs, T., Schmidt, M., Schwalm, C. R., Shekhar, A., Silberstein, R., Silveira,
958 M. L., Spano, D., Tagesson, T., Tramontana, G., Trotta, C., Turco, F., Vesala, T., Vincke, C.,
959 Vitale, D., Vivoni, E. R., Wang, Y., Woodgate, W., Yepez, E. A., Zhang, J., Zona, D., and Jung,
960 M.: X-BASE: the first terrestrial carbon and water flux products from an extended data-driven
961 scaling framework, *FLUXCOM-X, Biogeosciences*, 21, 5079-5115,

Formatted: Font: Italic

Deleted: 2008.

Deleted: Hydrol

Deleted: Syst Sci

Formatted: Font: Italic

Formatted: Font: Italic

Formatted: Font: Italic

Deleted: Sci

Formatted: Font: Italic

Formatted: Font: Italic

Formatted: Font: Italic

Formatted: Font: Italic

Deleted: FAO2023

Formatted: Font: Italic

967 <https://doi.org/10.5194/bg-21-5079-2024>, 2024.

968 Nogueira, M., Boussetta, S., Balsamo, G., Albergel, C., Trigo, I. F., Johannsen, F., Miralles, D.
969 G., and Dutra, E.: Upgrading Land-Cover and Vegetation Seasonality in the ECMWF Coupled
970 System: Verification With FLUXNET Sites, METEOSAT Satellite Land Surface
971 Temperatures, and ERA5 Atmospheric Reanalysis, *Journal of Geophysical Research:
972 Atmospheres*, 126, e2020JD034163, <https://doi.org/10.1029/2020JD034163>, 2021.

973 O, S. and Orth, R.: Global soil moisture data derived through machine learning trained with in-
974 situ measurements, *Scientific Data*, 8, 170, <https://doi.org/10.1038/s41597-021-00964-1>,
975 2021.

976 O'Gorman, P. A.: Contrasting responses of mean and extreme snowfall to climate change,
977 *Nature*, 512, 416-418, <https://doi.org/10.1038/nature13625>, 2014.

978 Oki, T. and Kanae, S.: Global hydrological cycles and world water resources, *Science*, 313,
979 1068-1072, <https://doi.org/10.1126/science.1128845>, 2006.

980 Pan, S. F., Pan, N. Q., Tian, H. Q., Friedlingstein, P., Sitch, S., Shi, H., Arora, V. K., Haverd, V.,
981 Jain, A. K., Kato, E., Lienert, S., Lombardozzi, D., Nabel, J. E. M. S., Otté, C., Poulter, B.,
982 Zaehle, S., and Running, S. W.: Evaluation of global terrestrial evapotranspiration using state-
983 of-the-art approaches in remote sensing, machine learning and land surface modeling,
984 *Hydrology and Earth System Sciences*, 24, 1485-1509, [https://doi.org/10.5194/hess-24-1485-](https://doi.org/10.5194/hess-24-1485-2020)
985 2020, 2020.

986 Pastorello, G., Trotta, C., Canfora, E., Chu, H., Christianson, D., Cheah, Y. W., Poindexter, C.,
987 Chen, J., Elbashandy, A., Humphrey, M., Isaac, P., Polidori, D., Reichstein, M., Ribeca, A.,
988 van Ingen, C., Vuichard, N., Zhang, L., Amiro, B., Ammann, C., Arain, M. A., Ardo, J.,
989 Arkebauer, T., Arndt, S. K., Arriga, N., Aubinet, M., Aurela, M., Baldocchi, D., Barr, A.,
990 Beamesderfer, E., Marchesini, L. B., Bergeron, O., Beringer, J., Bernhofer, C., Berveiller, D.,
991 Billesbach, D., Black, T. A., Blanken, P. D., Bohrer, G., Boike, J., Bolstad, P. V., Bonal, D.,
992 Bonnefond, J. M., Bowling, D. R., Bracho, R., Brodeur, J., Brummer, C., Buchmann, N.,
993 Burban, B., Burns, S. P., Buysse, P., Cale, P., Cavagna, M., Cellier, P., Chen, S., Chini, I.,
994 Christensen, T. R., Cleverly, J., Collalti, A., Consalvo, C., Cook, B. D., Cook, D., Coursolle,
995 C., Cremonese, E., Curtis, P. S., D'Andrea, E., da Rocha, H., Dai, X., Davis, K. J., Cinti, B.,
996 Grandcourt, A., Ligne, A., De Oliveira, R. C., Delpierre, N., Desai, A. R., Di Bella, C. M.,
997 Tommasi, P. D., Dolman, H., Domingo, F., Dong, G., Dore, S., Duce, P., Dufrene, E., Dunn,
998 A., Dusek, J., Eamus, D., Eichelmann, U., ElKhidir, H. A. M., Eugster, W., Ewenz, C. M.,
999 Ewers, B., Famulari, D., Fares, S., Feigenwinter, I., Feitz, A., Fensholt, R., Filippa, G.,
1000 Fischer, M., Frank, J., Galvagno, M., Gharun, M., Gianelle, D., Gielen, B., Gioli, B., Gitelson,
1001 A., Goded, I., Goeckede, M., Goldstein, A. H., Gough, C. M., Goulden, M. L., Graf, A.,
1002 Griebel, A., Gruening, C., Grunwald, T., Hammerle, A., Han, S., Han, X., Hansen, B. U.,
1003 Hanson, C., Hatakka, J., He, Y., Hehn, M., Heinesch, B., Hinko-Najera, N., Hortnagl, L.,
1004 Hutley, L., Ibrom, A., Ikawa, H., Jackowicz-Korczynski, M., Janous, D., Jans, W., Jassal, R.,
1005 Jiang, S., Kato, T., Khomik, M., Klatt, J., Knohl, A., Knox, S., Kobayashi, H., Koerber, G.,
1006 Kolle, O., Kosugi, Y., Kotani, A., Kowalski, A., Kruijt, B., Kurbatova, J., Kutsch, W. L.,
1007 Kwon, H., Launiainen, S., Laurila, T., Law, B., Leuning, R., Li, Y., Liddell, M., Limousin, J.
1008 M., Lion, M., Liska, A. J., Lohila, A., Lopez-Ballesteros, A., Lopez-Blanco, E., Loubet, B.,
1009 Loustau, D., Lucas-Moffat, A., Luers, J., Ma, S., Macfarlane, C., Magliulo, V., Maier, R.,
1010 Mammarella, I., Manca, G., Marcolla, B., Margolis, H. A., Marras, S., Massman, W.,
1011 Mastepanov, M., Matamala, R., Matthes, J. H., Mazzenga, F., McCaughey, H., McHugh, I.,
1012 McMillan, A. M. S., Merbold, L., Meyer, W., Meyers, T., Miller, S. D., Minerbi, S., Moderow,

Deleted: NOAA National Centers for Environmental Information: ETOPO 2022 15 Arc-Second Global Relief Model, 10.25921/fd45-gt74, 2022.

Deleted: J Geophys Res Atmos

Formatted: Font: Italic

Formatted: Font: Italic

Formatted: Font: Italic

Formatted: Font: Italic

1017 U., Monson, R. K., Montagnani, L., Moore, C. E., Moors, E., Moreaux, V., Moureaux, C.,
1018 Munger, J. W., Nakai, T., Neiryneck, J., Nesic, Z., Nicolini, G., Noormets, A., Northwood, M.,
1019 Nosoetto, M., Nouvellon, Y., Novick, K., Oechel, W., Olesen, J. E., Ourcival, J. M., Papuga, S.
1020 A., Parmentier, F. J., Paul-Limoges, E., Pavelka, M., Peichl, M., Pendall, E., Phillips, R. P.,
1021 Pilegaard, K., Pirk, N., Posse, G., Powell, T., Prasse, H., Prober, S. M., Rambal, S., Rannik,
1022 U., Raz-Yaseef, N., Reibmann, C., Reed, D., Dios, V. R., Restrepo-Coupe, N., Reverter, B. R.,
1023 Roland, M., Sabbatini, S., Sachs, T., Saleska, S. R., Sanchez-Canete, E. P., Sanchez-Mejia, Z.
1024 M., Schmid, H. P., Schmidt, M., Schneider, K., Schrader, F., Schroder, I., Scott, R. L., Sedlak,
1025 P., Serrano-Ortiz, P., Shao, C., Shi, P., Shironya, I., Siebicke, L., Sigut, L., Silberstein, R.,
1026 Sirca, C., Spano, D., Steinbrecher, R., Stevens, R. M., Sturtevant, C., Suyker, A., Tagesson, T.,
1027 Takanashi, S., Tang, Y., Tapper, N., Thom, J., Tomassucci, M., Tuovinen, J. P., Urbanski, S.,
1028 Valentini, R., van der Molen, M., van Gorsel, E., van Huissteden, K., Varlagin, A., Verfaillie,
1029 J., Vesala, T., Vincke, C., Vitale, D., Vygodskaya, N., Walker, J. P., Walter-Shea, E., Wang, H.,
1030 Weber, R., Westermann, S., Wille, C., Wofsy, S., Wohlfahrt, G., Wolf, S., Woodgate, W., Li,
1031 Y., Zampedri, R., Zhang, J., Zhou, G., Zona, D., Agarwal, D., Biraud, S., Torn, M., and
1032 Papale, D.: The FLUXNET2015 dataset and the ONEFlux processing pipeline for eddy
1033 covariance data, *Scientific Data*, 7, 225, <https://doi.org/10.1038/s41597-020-0534-3>, 2020.

1034 Reichle, R. H., Liu, Q., Koster, R. D., Crow, W. T., De Lannoy, G. J. M., Kimball, J. S.,
1035 Ardizzone, J. V., Bosch, D., Colliander, A., Cosh, M., Kolassa, J., Mahanama, S. P., Prueger,
1036 J., Starks, P., and Walker, J. P.: Version 4 of the SMAP Level-4 Soil Moisture Algorithm and
1037 Data Product, *Journal of Advances in Modeling Earth Systems*, 11, 3106-3130,
1038 <https://doi.org/10.1029/2019ms001729>, 2019.

1039 Rodell, M., Houser, P. R., Jambor, U., Gottschalck, J., Mitchell, K., Meng, C. J., Arsenault, K.,
1040 Cosgrove, B., Radakovich, J., Bosilovich, M., Entin, J. K., Walker, J. P., Lohmann, D., and
1041 Toll, D.: The Global Land Data Assimilation System, *Bulletin of the American Meteorological
1042 Society*, 85, 381-394, <https://doi.org/10.1175/bams-85-3-381>, 2004.

1043 Rui, H., Beaudoin, H., and Loeser, C.: README Document for NASA GLDAS Version 2 Data
1044 Products, 2022.

1045 Ruiz-Vásquez, M., O. S., Brenning, A., Koster, R. D., Balsamo, G., Weber, U., Arduini, G.,
1046 Bastos, A., Reichstein, M., and Orth, R.: Exploring the relationship between temperature
1047 forecast errors and Earth system variables, *Earth System Dynamics*, 13, 1451-1471,
1048 <https://doi.org/10.5194/esd-13-1451-2022>, 2022.

1049 Ruiz-Vásquez, M., O. S., Arduini, G., Boussetta, S., Brenning, A., Bastos, A., Koirala, S.,
1050 Balsamo, G., Reichstein, M., and Orth, R.: Impact of Updating Vegetation Information on
1051 Land Surface Model Performance, *Journal of Geophysical Research: Atmospheres*, 128,
1052 <https://doi.org/10.1029/2023jd039076>, 2023.

1053 Running, S., Mu, Q., Zhao, M., and Moreno, A.: MODIS/Terra Net Evapotranspiration Gap-
1054 Filled 8-Day L4 Global 500m SIN Grid V061,
1055 <https://doi.org/10.5067/MODIS/MOD16A2GF.061>, 2021.

1056 Schneider, U., Hänsel, S., Finger, P., Rustemeier, E., and Ziese, M.: GPCC Full Data Monthly
1057 Product Version 2022 at 0.25°: Monthly Land-Surface Precipitation from Rain-Gauges built
1058 on GTS-based and Historical Data, https://doi.org/10.5676/DWD_GPCC/FD_M_V2022_025,
1059 2022.

1060 Slivinski, L. C., Compo, G. P., Sardeshmukh, P. D., Whitaker, J. S., McColl, C., Allan, R. J.,
1061 Brohan, P., Yin, X., Smith, C. A., Spencer, L. J., Vose, R. S., Rohrer, M., Conroy, R. P.,
1062 Schuster, D. C., Kennedy, J. J., Ashcroft, L., Brönnimann, S., Brunet, M., Camuffo, D.,

Deleted: Sci

Formatted: Font: Italic

Deleted: J Adv Model

Deleted: Sy

Formatted: Font: Italic

Formatted: Font: Italic

Deleted:

Moved down [6]: Ruiz-Vásquez, M., O. S., Arduini, G., Boussetta, S.,

Moved down [7]: Brenning, A., Bastos, A., Koirala, S., Balsamo, G., Reichstein, M., and Orth, R.: Impact of

Deleted: updating vegetation information on land surface model performance, 10.22541/essoar.168182273.38487150/v1, 2023.

Formatted: Font: Italic

Moved (insertion) [6]

Moved (insertion) [7]

Deleted:

Deleted:

1076 Comes, R., Cram, T. A., Domínguez-Castro, F., Freeman, J. E., Gergis, J., Hawkins, E., Jones,
1077 P. D., Kubota, H., Lee, T. C., Lorrey, A. M., Luterbacher, J., Mock, C. J., Przybylak, R. K.,
1078 Pudmenzky, C., Slonosky, V. C., Tinz, B., Trewin, B., Wang, X. L., Wilkinson, C., and Wood,
1079 K.: An Evaluation of the Performance of the Twentieth Century Reanalysis Version 3, *Journal*
1080 *of Climate*, 34, 1417-1438, <https://doi.org/10.1175/Jcli-D-20-0505.1>, 2021.

1081 Sun, Q. H., Miao, C. Y., Duan, Q. Y., Ashouri, H., Sorooshian, S., and Hsu, K. L.: A Review of
1082 Global Precipitation Data Sets: Data Sources, Estimation, and Intercomparisons, *Reviews of*
1083 *Geophysics*, 56, 79-107, <https://doi.org/10.1002/2017rg000574>, 2018.

1084 Tang, G. Q., Clark, M. P., and Papalexiou, S. M.: EM-Earth The Ensemble Meteorological
1085 Dataset for Planet Earth, *Bulletin of the American Meteorological Society*, 103, E996-E1018,
1086 <https://doi.org/10.1175/Bams-D-21-0106.1>, 2022.

1087 Tang, R. L., Peng, Z., Liu, M., Li, Z. L., Jiang, Y. Z., Hu, Y. X., Huang, L. X., Wang, Y. Z.,
1088 Wang, J. R., Jia, L., Zheng, C. L., Zhang, Y. Q., Zhang, K., Yao, Y. J., Chen, X. L., Xiong, Y.
1089 J., Zeng, Z. Z., and Fisher, J. B.: Spatial-temporal patterns of land surface evapotranspiration
1090 from global products, *Remote Sensing of Environment*, 304,
1091 <https://doi.org/10.1016/j.rse.2024.114066>, 2024.

1092 Vargas Godoy, M. R., Markonis, Y., Thomson, J. R., Simões Ballarin, A., Perri, S., Miao, C.,
1093 Sun, Q., Hanel, M., Papalexiou, S. M., Kummerow, C., Oki, T., and Molini, A.: Which
1094 Precipitation Dataset to Choose for Hydrological Studies of the Terrestrial Water Cycle?,
1095 *Bulletin of the American Meteorological Society*, 106, E2000-E2016,
1096 <https://doi.org/10.1175/bams-d-24-0306.1>, 2025.

1097 Wang, H., Liu, J., Klaar, M., Chen, A., Gudmundsson, L., and Holden, J.: Anthropogenic climate
1098 change has influenced global river flow seasonality, *Science*, 383, 1009-1014,
1099 <https://doi.org/10.1126/science.adi9501>, 2024.

1100 Wang-Erlandsson, L., Tobian, A., van der Ent, R. J., Fetzer, I., te Wierik, S., Porkka, M., Staal,
1101 A., Jaramillo, F., Dahlmann, H., Singh, C., Greve, P., Gerten, D., Keys, P. W., Gleeson, T.,
1102 Cornell, S. E., Steffen, W., Bai, X. M., and Rockstrom, J.: A planetary boundary for green
1103 water, *Nature Reviews Earth & Environment*, 3, 380-392, [https://doi.org/10.1038/s43017-022-](https://doi.org/10.1038/s43017-022-00287-8)
1104 00287-8, 2022.

1105 Xie, P. P. and Arkin, P. A.: Global precipitation: A 17-year monthly analysis based on gauge
1106 observations, satellite estimates, and numerical model outputs, *Bulletin of the American*
1107 *Meteorological Society*, 78, 2539-2558, [https://doi.org/10.1175/1520-](https://doi.org/10.1175/1520-0477(1997)078<2539:Gpayma>2.0.Co;2)
1108 0477(1997)078<2539:Gpayma>2.0.Co;2, 1997.

1109 Xie, P. P., Chen, M., and Shi, W.: CPC unified gauge-based analysis of global daily precipitation,
1110 24th Conf. on Hydrology, Atlanta, GA, Amer. Meteor. Soc., 2010

1111 Xie, P. P., Joyce, R., Wu, S. R., Yoo, S. H., Yarosh, Y., Sun, F. Y., and Lin, R.: Reprocessed, Bias-
1112 Corrected CMORPH Global High-Resolution Precipitation Estimates from 1998, *Journal of*
1113 *Hydrometeorology*, 18, 1617-1641, <https://doi.org/10.1175/Jhm-D-16-0168.1>, 2017.

1114 Yang, Y. T., Roderick, M. L., Guo, H., Miralles, D. G., Zhang, L., Fatichi, S., Luo, X. Z., Zhang,
1115 Y. Q., McVicar, T. R., Tu, Z. Y., Keenan, T. F., Fisher, J. B., Gan, R., Zhang, X. Z., Piao, S. L.,
1116 Zhang, B. Q., and Yang, D. W.: Evapotranspiration on a greening Earth, *Nature Reviews Earth*
1117 *& Environment*, 4, 626-641, <https://doi.org/10.1038/s43017-023-00464-3>, 2023.

1118 Yao, Y. J., Liang, S. L., Li, X. L., Hong, Y., Fisher, J. B., Zhang, N. N., Chen, J. Q., Cheng, J.,
1119 Zhao, S. H., Zhang, X. T., Jiang, B., Sun, L., Jia, K., Wang, K. C., Chen, Y., Mu, Q. Z., and
1120 Feng, F.: Bayesian multimodel estimation of global terrestrial latent heat flux from eddy
1121 covariance, meteorological, and satellite observations, *Journal of Geophysical Research:*

Formatted: Font: Italic

Formatted: Font: Italic

Formatted: Font: Italic

Formatted: Font: Italic

Formatted: Font: Italic

Formatted: Font: Italic

Formatted: Font: Italic

Formatted: Font: Italic

Formatted: Font: Italic

Deleted: J Geophys Res-Atmos

1123 [Atmospheres](https://doi.org/10.1002/2013jd020864), 119, 4521-4545, <https://doi.org/10.1002/2013jd020864>, 2014.

1124 Zarei, M. and Destouni, G.: A global multi catchment and multi dataset synthesis for water fluxes
 1125 and storage changes on land, *Scientific Data*, 11, 1333, [https://doi.org/10.1038/s41597-024-](https://doi.org/10.1038/s41597-024-04203-1)
 1126 04203-1, 2024.

1127 Zeri, M., Costa, J., Urbano, D., Cuartas, L., Ivo, A., Marengo, J., and Alvala, R.: A soil moisture
 1128 dataset over the Brazilian semiarid region, Mendeley Data Version, 2, 2020.

1129 Zhang, W. X., Zhou, T. J., and Wu, P. L.: Anthropogenic amplification of precipitation variability
 1130 over the past century, *Science*, 385, 427-432, <https://doi.org/10.1126/science.adp0212>, 2024a.

1131 [Zhang, Y., Pan, M., and Wood, E. F.: On Creating Global Gridded Terrestrial Water Budget
 1132 Estimates from Satellite Remote Sensing, in: Remote Sensing and Water Resources, *Space
 1133 Sciences Series of ISSI*, 59-78, \[https://doi.org/10.1007/978-3-319-32449-4_4\]\(https://doi.org/10.1007/978-3-319-32449-4_4\), 2016.](https://doi.org/10.1007/978-3-319-32449-4_4)

1134 Zhang, Y. Q., Kong, D. D., and Xu, Z. W.: PML_V2 global evapotranspiration and gross primary
 1135 production (2000.02-2023.12), Zenodo, <https://doi.org/10.5281/zenodo.10647617>, 2024b.

1136 Zhang, Y. Q., Kong, D. D., Gan, R., Chiew, F. H. S., McVicar, T. R., Zhang, Q., and Yang, Y. T.:
 1137 Coupled estimation of 500 m and 8-day resolution global evapotranspiration and gross
 1138 primary production in 2002-2017, *Remote Sensing of Environment*, 222, 165-182,
 1139 <https://doi.org/10.1016/j.rse.2018.12.031>, 2019.

Deleted: Sci

Formatted: Font: Italic

Formatted: Font: Italic

Formatted: Font: Italic